Palestine Journal of Mathematics

Vol 14(4)(2025) , 298–328

Constrained Optimal Control Problem Applied to Vaccination for COVID-19 Epidemic

Chiraz Trabelsi, Rim Amami, Walid Ben Aribi and Hani Abidi

Communicated by: Sabrina Streipert

MSC 2010 Classifications: Primary 49J15, 49K15, 92D30; Secondary 34H05.

Keywords: Covid-19 Epidemic, Extended SEAIR, Vaccine, Ordinary differential equations, Optimal control problem, penalty method.

The authors would like to thank Professor Monique Pontier for her constructive comments and suggestions, which helped improve the quality of our work.

Corresponding Author: R. Amami

Abstract In this study, we propose a dynamic mathematical model framework governed by a system of differential equations that integrates COVID-19 outbreaks. We extend the standard SEAIR model to incorporate the vaccination component. We analyze the existence and uniqueness of the solution, compute the basic reproduction number $\mathcal{R}_0$, and study the equilibrium state's local stability.
We formulate an optimal control problem to minimize the number of infected individuals while considering intervention costs. Our optimal control problem integrates two realistic constraints: total vaccine administration and maximum daily vaccine administration. We use a penalty method to handle these constraints to convert this problem to a more familiar form. We approximate the obtained constrained optimization problem and derive an optimality system that characterizes the optimal control. Finally, we perform numerical simulations using the reported data on COVID-19 infections and vaccination in France to compare the optimal intervention strategies under different settings.

1 Introduction

Mathematical modeling is an indispensable tool in studying and controlling infectious diseases, providing a robust framework to simulate and understand the spread and impact of pathogens within populations. The importance of mathematical modeling in infectious diseases lies in its ability to predict outbreaks, assess the potential effectiveness of public health interventions, and guide policy decisions. For instance, during the COVID-19 pandemic, models were instrumental in projecting case numbers, evaluating the impact of social distancing and vaccination campaigns, and optimizing resource allocation. Consequently, mathematical modeling not only enhances our comprehension of disease mechanics but also equips health authorities with evidence-based insights to mitigate the spread of infections and minimize public health impacts. Among the authors who provide mathematical modeling in infectious diseases, we cite the authors in [33] who are focused on the modeling and numerical solution of the dynamical model of Typhoid Fever by using protected, susceptible, exposed, infected, and treated compartments under Atangana Baleanu Caputo fractional order derivative.
Furthermore, a mathematical model for the pine wilt disease dynamics is considered in [2, 32].

Appearing in 2019 in Wuhan, COVID-19 very quickly turned out to be a serious health problem around the world, with catastrophic consequences for the evolution of humankind. All statistics data about coronavirus COVID-19 comes from the World Health Organization, Johns Hopkins CSSE, and Worldometers. Charts include the number of infected, deaths, and recovered people.

There is now no medicine or specific treatment for COVID-19, and most countries have been relying on non-pharmaceutical interventions, such as wearing face masks, washing hands taking care of personal hygiene, physical distancing, rapid-test and even more partial or total lockdown to curtail the spread of the disease. Therefore the study of the novel coronavirus has relatively attracted some importance in mathematical epidemiology due to its seriousness and the way it spreads worldwide.

For instance, several models have been proposed to provide insight into the effect that inoculation of a certain portion of the population will have on the dynamics of the COVID-19 pandemic.

The first epidemiological model, the SIR (Susceptible-Infectious-Recovered) model, was introduced by Kermack and McKendrick in 1927. This model assumes that the population is divided into three compartments: Susceptible, Infected, and Recovered, with lifelong immunity to the disease. Numerous significant extensions have since been developed from the classic SIR model to create more complex models, making epidemic modeling more realistic. These advancements have improved the understanding and management of infectious diseases within the population. To investigate the spread of coronavirus in Pakistan, the authors in [4] develop the SEIR time fractional model with the newly, developed fractional operator of Atangana-Baleanu. In the same study, see [3, 24].

The main contribution in [25] is to introduce a comprehensive understanding of the SARS-CoV-2 pandemic in African countries (Madagascar, Senegal, and Tunisia), shedding light on the influence of immunity and viral variants on disease dynamics. The findings of this study can provide data for improving public health strategies and interventions tailored to the unique context of African countries.

The author in [10] analyzes the convergence of difference approximations for an optimal control problem governed by a quasilinear parabolic equation, with controls in the conductivity coefficient, boundary conditions, and source terms. It establishes stability estimates for the discrete approximation problem (DAP) and proves the convergence of the method for the associated optimal control problem.

The authors in [29] apply optimal control theory to determine optimal strategies for the implementation of non-pharmaceutical interventions to control COVID-19. The studied model was calibrated to data from the USA and focused the analysis on optimal controls from May 2020 through December 2021.

The study in [1] formulates an SIQR-W mathematical model to analyze COVID-19 dynamics under health education campaigns and quarantine controls, demonstrating that efficient health education significantly reduces infection rates. Theoretical analysis includes boundedness, equilibrium stability, and numerical simulations, highlighting the critical role of public awareness in epidemic mitigation.

The importance of the isolation strategy was emphasized in [8] to reduce the infection of COVID-19. The authors prove the existence and uniqueness of a global positive solution for a COVID-19 stochastic model with an isolation strategy. Some numerical simulations are presented to illustrate the theoretical results.

Many mathematical models conclude that lockdown is the best way to reduce the spread of COVID-19 effectively among all the aforementioned control strategies [21]. However, partial or total lockdown strategies are very risky for a country's economic stability, therefore some suggested mathematical models focused on analyzing the effect of COVID-19 rapid-test as an alternative to suppress the spread of COVID-19 [6, 35].

However, these measures have been not an effective protection to mitigate the pandemic globally. To bring this pandemic to an end, a large share of the world needs to be immune to the virus. The safest way to achieve this is with a vaccine. Within less than 12 months after the beginning of the COVID-19 pandemic, several research teams rose to the challenge and developed vaccines that protect from SARS-CoV-2.

Among other studies, [11] applies optimal control theory to suggest the most effective mitigation strategy to minimize the number of individuals who become infected during infection, while efficiently balancing vaccination and treatment within the models. The analysis of the SIR model is presented here, including the proof of uniqueness and the existence of the optimal control solutions.

The motivation of this study is derived from the work [9], who adopt a more modeling approach based on optimal control theory to determine the best strategy to implement until vaccine deployment. Given the evolution of the COVID-19 epidemic, we are convinced that the classic SEAIR model could be improved to consider the progression of the epidemic during the vaccination campaign. What model can be implemented to consider the effect of vaccination? Once the model is studied, can we identify the optimal strategy considering constraints such as the maximum daily number of vaccines and vaccine coverage?

Therefore, in the present study, we incorporate the vaccination component to the model in [9], to derive an extended SEAIR model to examine the effectiveness of the COVID-19 jabs which are currently being deployed to many countries to help combat the raging pandemic situation. In the same area, the authors in [27] propose and analyze an extended SEIARD model with vaccination to examine the effectiveness of the COVID-19 jabs which are currently being deployed to many countries to help combat the raging pandemic situation. Some numerical simulations are achieved using reported data on COVID-19 infections and vaccination in Mexico.

This paper is composed of five sections. We first present in Section 2, the structure of our epidemiological model, precisely we present the equations and assumptions of the extended SEAIR model with vaccination. Section 3 is devoted to analyzing the existence and uniqueness of the solution, we compute the basic reproduction number $\mathcal{R}_0$ as well as studying the stability of the studied system. In Section 4, we introduce the objective function and a reformulation of the optimal control problem to minimize the incidence satisfying the constraints of the total and maximum daily vaccine administration and we derive the optimality condition. We use the penalty method to approximate this constrained optimization problem and derive an optimality system that characterizes the optimal control. In Section 5, we carry out numerical simulations using reported data on COVID-19 infections and vaccination in France and conclude with a summary.

2 Model formulation

The model describes the epidemic dynamics of COVID-19 in a population after vaccine deployment and is an extension of the standard SEAIR model incorporating a temporary protection vaccine compartment to the model [9], regardless of the disease severity whether mild or severe infections. To develop the mathematical model, we divide our population into two sub-populations. The first sub-population consists of the unvaccinated individuals categorized into several states: susceptible (S), representing those who are uninfected and vulnerable to the circulating virus; latent (E), or the exposed state characterizes infected individuals who are in the early stages of infection but not yet symptomatic (incubation period); asymptomatic infectious (A), describing those who are infected and capable of spreading the virus while remaining asymptomatic; symptomatic infectious (I), the infected state characterizes infected and infectious symptomatic individuals; immune (R), representing those who have recovered and gained immunity; and death (D), the deceased state represents individuals who have died as a result of the disease.

The second one, is the vaccinated population (individuals who have received one, two, or three doses of the vaccine), mainly the temporary protection vaccine (V), which classifies vaccinated individuals into principle key compartments:

- Vaccine susceptible (VS).
- Vaccine latent (VE): vaccine infected but asymptomatic and not infectious.
- Vaccine asymptomatic infectious (VA).
- Vaccine symptomatic infectious (VI).

- Immune (VR) or Death (D).

The main variables and parameters of the proposed model are shown in the following flow diagram, see Figure 1, and listed in Table 1.

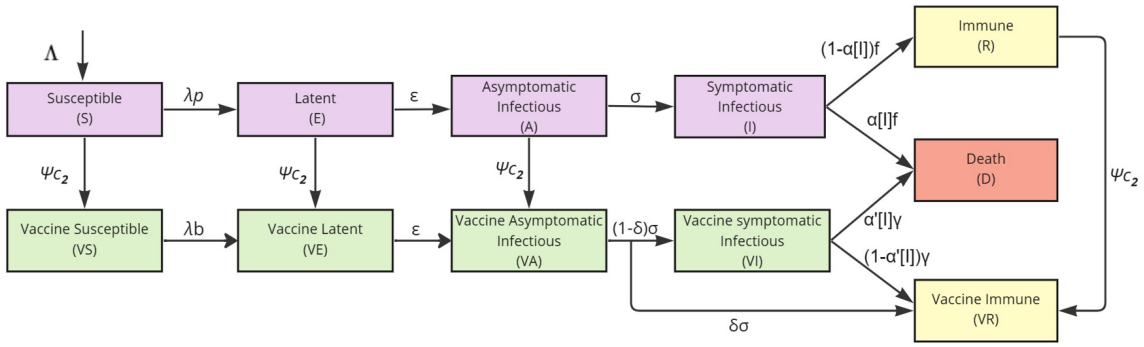

Figure 1. Flow diagram for the SEAIR model with vaccination compartments.

We will denote by $N(t)$ the total population size at time t which is given by

$$N(t) = S(t) + E(t) + A(t) + I(t) + R(t) + VS(t) + VE(t) + VA(t) + VI(t) + VR(t).$$

We denote by c_1 the control effort which represents the percentage of reduction in transmission due to public health measures at time t, and β_A, β_I are asymptomatic and symptomatic transmission rates respectively. Susceptible individuals become exposed by contact with asymptomatic infectious individuals at a rate β_A and by contact with symptomatic infectious individuals at a rate β_I. We assume that the incidence rate depends on the number of susceptible and infectious individuals. The transmission function is always positive, continuous, differentiable, and strictly increasing for all $S \geq 0$, $A \geq 0$, and $I \geq 0$. Following the simple form of the mass action law, the incidence can be expressed as:

$$\beta_A SA + \beta_I SI.$$

By incorporating a time-dependent control function $c_1(t)$, which represents the effect of interventions such as social distancing or lockdown measures, the transmission rate can be reformulated as follows:

$$\lambda = (1 - c_1(t))(\beta_A A + \beta_I I).$$

This equation formally defines the force of infection in [9], highlighting the impact of control measures on disease transmission. The term $(1 - c_1(t))$ dynamically adjusts the transmission rate over time, while $\beta_A A$ and $\beta_I I$ represent the contributions of asymptomatic individuals and symptomatic individuals, respectively, to the spread of the disease. A proportion p of exposed individuals (λS) move to the asymptomatic infection class at a rate ϵ. We assume that asymptomatic infectious individuals become symptomatic infectious at rate σ.

In our case, we have neglected the direct transfer from asymptomatic to cured individuals, and assume that asymptomatic individuals become symptomatic at a rate σ. This approach reflects how these individuals become visible to health authorities, enabling them to be isolated and treated appropriately. Furthermore, as epidemiological data is more complete for symptomatic individuals, focusing on this transition improves data alignment and analysis accuracy. In addition, modeling this transition provides a better understanding of transmission dynamics, especially as symptomatic individuals often have higher transmission rates. He, X., et al., in [12], examine the

dynamics of viral shedding and the transmissibility of COVID-19, highlighting the importance of the symptomatic phase for detection and isolation. The authors in [26] focus on the prevalence of asymptomatic infections and their role in transmission, compared to symptomatic individuals. The study in [16] highlights the contribution of undocumented infections (often asymptomatic) to the spread of the virus and underscores the necessity of models aligned with symptomatic data for more accurate epidemiological analysis.
Infective individuals leave the compartment at the rate $(1-\alpha[I])$ with the fraction f recovering from disease. In contrast, with the rest dying of infection, we assume the disease-induced mortality rate α to be a step function as follows:

$$\alpha[I] = \begin{cases} \alpha_{min} & \text{if } I < I^*, \\ \alpha_{max} & \text{if } I \geq I^*. \end{cases}$$

and I^* is the total number of infected hosts in the healthcare system, or simply the healthcare capacity and α bound disease-induced mortality rate.

Since an antibody test is not required or recommended before getting the COVID-19 vaccination, we assume the time-dependent control function $c_2(t)$ measures the rate at which Susceptible, Latent, Asymptomatic infectious and recovered individuals are vaccinated with vaccine efficacy ψ. As the vaccine does not completely remove the infection, we assume that a proportion b, $b \ll p$, of exposed vaccine individuals (λVS) move to asymptomatic infection at the same rate ϵ. A proportion δ of vaccine asymptomatic infectious individuals become recovered at the rate σ, while the remainder $(1-\delta)$ move to vaccine Symptomatic infection class at the same rate σ and recovered at rate $\gamma(1-\alpha'[I])$ with $\alpha' \ll \alpha$, denotes the disease-induced mortality for vaccinated individuals, whereas the rest dying of infection.

We also assume that natural mortality increases because of hospital saturation for the whole population level. We capture this using the following step function for the mortality rate μ,

$$\mu[I] = \begin{cases} 0 & \text{if } I < I^*, \\ \mu & \text{if } I \geq I^*. \end{cases}$$

with μ the natural mortality rate with hospital saturation.

The principal parameters used throughout this paper and their interpretation are as follows:

- μ : natural mortality rate with hospital saturation.
- α, α' : bounds disease induced mortality rate with $\alpha' \ll \alpha$.
- $c_1 \in [0,1]$ control effort. The percentage of reduction in transmission due to public health measures at the time is t.
- $c_2 \in [0,1]$ control effort. The time-dependent control function $c_2(t)$ measures the rate at which susceptible individuals are vaccinated.
- Force infection: $\lambda = (1-c_1(t))(\beta_A A + \beta_I I)$ where $\begin{cases} \beta_I & = & \text{symptotic transmission rate} \\ \beta_A & = & \text{asymptotic transmission rate} \end{cases}$
- Λ : a constant defined by the number of people being recruited into the population through migration or birth.
- ψ : susceptible, latent, asymptomatic, and recovered individuals are vaccinated with vaccine efficacy ψ.
- p : proportion of infections unvaccinated individuals.
- b : proportion of infections vaccinated individuals (It can be considered too as the loss of vaccine protection).
- ϵ : waiting rate to viral shedding.
- σ : waiting rate to symptom onset.

- f : recovery rate from infections unvaccinated individuals.
- γ : recovery rate from infections vaccinated individuals.
- δ : proportion of recovered among vaccine asymptomatic infectious individuals.

Setting $x'(t) = \dfrac{dx(t)}{dt}$, hence our model (1) is described by the following system of ODEs :

$$\begin{cases} S'(t) = \Lambda - \lambda p S(t) - \mu[I]S(t) - \psi c_2(t)S(t), \\ E'(t) = \lambda p S(t) - (\epsilon + \mu[I])E(t) - \psi c_2(t)E(t), \\ A'(t) = \epsilon E(t) - (\sigma + \mu[I])A(t) - \psi c_2(t)A(t), \\ I'(t) = \sigma A(t) - (f + \mu[I])I(t), \\ R'(t) = (1-\alpha[I])fI(t) - \mu[I]R(t) - \psi c_2(t)R(t), \\ VS'(t) = \psi c_2(t)S(t) - (\lambda b + \mu[I])VS(t), \\ VE'(t) = \psi c_2(t)E(t) + \lambda b VS(t) - (\epsilon + \mu[I])VE(t), \\ VA'(t) = \psi c_2(t)A(t) + \epsilon VE(t) - (\sigma + \mu[I])VA(t), \\ VI'(t) = (1-\delta)\sigma VA(t) - (\gamma + \mu[I])VI(t), \\ VR'(t) = \psi c_2(t)R(t) + \delta\sigma VA(t) + (1-\alpha'[I])\gamma VI(t) - \mu[I]VR(t), \\ D'(t) = \alpha[I]fI(t) + \alpha'[I]\gamma VI(t) + \mu[I]N(t). \end{cases} \tag{2.1}$$

with the following initial conditions

$$\begin{aligned} &S(0) = S_0 = N_0 - (I_0 + E_0 + A_0 + R_0 + D_0) \geq 0, \\ &E(0) = E_0 \geq 0, \quad A(0) = A_0 \geq 0, \quad I(0) = I_0 \geq 0, \quad R(0) = R_0 \geq 0, \\ &VS(0) = 0, \quad VE(0) = 0, \quad VA(0) = 0, \quad VI(0) = 0, \quad VR(0) = 0, \\ &D(0) = D_0 \geq 0, \quad N(0) = N_0 \geq 0. \end{aligned} \tag{2.2}$$

3 Analysis of the Extended SEAIR model (2.1) with constant controls

In this section, we analyze the existence and uniqueness of the solution, compute the basic reproduction number $\mathcal{R}_0$, and study the stability of the nonlinear system of ODEs (2.1) with the initial conditions (2.2).

The following theorem ensures that the solution of equations (2.1) exists and is unique.

Theorem 3.1. *If* $\dfrac{\Lambda}{\mu[I] + \alpha[I]f + \alpha'[I]\gamma} \leq N(0) \leq \dfrac{\Lambda}{\mu[I]}$, *then, the system (2.1) with initial conditions (2.2) admits a unique solution and the solution remains in the following region:*

$$\Gamma = \{(S, \ldots, R, VS, \ldots, VR, D) \in \mathbb{R}^{11} | S \geq 0, \ldots, R \geq 0, VS \geq 0, \ldots, VR \geq 0, D \geq 0\}.$$

Proof. First of all, we note that the variable D does not appear in the first equations of the model (2.1), so it suffices to analyze the behavior without the seventh equation.
The model (2.1) without the sixth equation can be written as follows $\dot{X}(t) = F(X(t))$, where

$$X(t) = (S(t), E(t), A(t), I(t), R(t), VS(t), VE(t), VA(t), VI(t), VR(t),$$

and $F \in C^{\infty}(\mathbb{R}^{10}_{+}, \mathbb{R})$.
Since the function F is locally Lipschitzian then there exists a unique maximal solution to the problem of Cauchy Lipschitz associated with our differential system for an initial condition

$$(S(0),\ E(0),\ A(0),\ I(0),\ R(0), VS(0),\ VE(0),\ VA(0),\ VI(0),\ VR(0)) \in \mathbb{R}^{10}_{+}.$$

Furthermore, we have:

$$\begin{cases} \dfrac{dS(t)}{dt}|_{S(t)=0} = \Lambda \geq 0, \\ \dfrac{dE(t)}{dt}|_{E(t)=0} = \lambda p S(t) \geq 0, \\ \dfrac{dA(t)}{dt}|_{A(t)=0} = \epsilon E(t) \geq 0, \\ \dfrac{dI(t)}{dt}|_{I(t)=0} = \sigma A(t) \geq 0, \\ \dfrac{dR(t)}{dt}|_{R(t)=0} = (1-\alpha[I]) f I(t) \geq 0, \\ \dfrac{dVS(t)}{dt}|_{VS(t)=0} = \psi c_2(t) S(t) \geq 0, \\ \dfrac{dVE(t)}{dt}|_{VE(t)=0} = \psi c_2(t) E(t) + \lambda b V S(t) \geq 0, \\ \dfrac{dVA(t)}{dt}|_{VA(t)=0} = \psi c_2(t) A(t) + \epsilon V E(t) \geq 0, \\ \dfrac{dVI(t)}{dt}|_{VI(t)=0} = (1-\delta)\sigma V A(t) \geq 0, \\ \dfrac{dVR(t)}{dt}|_{VR(t)=0} = \psi c_2(t) R(t) + \delta\sigma V A(t) + (1-\alpha'[I])\gamma V I(t) \geq 0. \end{cases}$$

Then the solution of the system (2.1) will be positive. In addition, thanks to the definition of Γ, we have

$$\frac{dN(t)}{dt} = \Lambda - \mu[I]N(t) - \alpha[I] f I(t) - \alpha'[I]\gamma V I(t)$$

$$\Lambda - \left(\mu[I] + \alpha[I]f + \alpha'[I]\gamma\right) N(t) \leq \frac{dN(t)}{dt} \leq -\mu[I]\left(N(t) - \frac{\Lambda}{\mu[I]}\right).$$

Then, according to the comparison theorem [5], we obtain,

$$N(t) \geq \frac{\Lambda}{\mu[I] + \alpha[I]f + \alpha'[I]\gamma} + \left(N(0) - \frac{\Lambda}{\mu[I] + \alpha[I]f + \alpha'[I]\gamma}\right) e^{-(\mu[I]+\alpha[I]f+\alpha'[I]\gamma)t}$$

$$N(t) \leq \frac{\Lambda}{\mu[I]} + \left(N(0) - \frac{\Lambda}{\mu[I]}\right) e^{-\mu[I]t}.$$

If $\frac{\Lambda}{\mu[I]+\alpha[I]f+\alpha'[I]\gamma} \leq N(0) \leq \frac{\Lambda}{\mu[I]}$, then, we get

$$\frac{\Lambda}{\mu[I] + \alpha[I]f + \alpha'[I]\gamma} \leq N(t) \leq \frac{\Lambda}{\mu[I]}.$$

Thus, the solution of the system (2.1) without the last equation remains in the positive region $\mathbb{R}^{10}_+$. Hence, the solution of the system (2.1) remains in the positive region Γ.
Finally, by the boundedness of $S(t), E(t), A(t), I(t), R(t), VS(t), VE(t), VA(t), VI(t)$ and $VR(t)$ we deduce that we have a global solution. □

In the following proposition, we'll compute the basic reproduction number, $\mathcal{R}_0$, which quantifies the average number of new infections caused by a single infected individual during their entire period of contagiousness in a fully susceptible population. According to Van Den Driessche [37], $\mathcal{R}_0$ is given by the spectral radius of the next-generation matrix, meaning it is equal to its largest eigenvalue.

Proposition 3.2. *The basic reproduction number of the system (2.1) with initial conditions (2.2) is*

$$\mathcal{R}_0 := \frac{p(1-c_1)S^*\left[\beta_A \epsilon(f + \mu[I]) + \beta_I \epsilon\sigma\right]}{(\epsilon + \mu[I] + \psi c_2)(\sigma + \mu[I] + \psi c_2)(f + \mu[I])},$$

where $S^* = \frac{\Lambda}{\mu[I]+\psi c_2}$.

Proof. The system (2.1) with initial conditions (2.2) has three disease compartments, namely E, A, and I. We can write

$$\begin{aligned}
\frac{dE}{dt} &= \mathcal{F}_1(X(t)) - \mathcal{V}_1(X(t)),\\
\frac{dA}{dt} &= \mathcal{F}_2(X(t)) - \mathcal{V}_2(X(t)),\\
\frac{dI}{dt} &= \mathcal{F}_3(X(t)) - \mathcal{V}_3(X(t)),\\
\frac{dVE}{dt} &= \mathcal{F}_4(X(t)) - \mathcal{V}_4(X(t)),\\
\frac{dVA}{dt} &= \mathcal{F}_5(X(t)) - \mathcal{V}_5(X(t)),\\
\frac{dVI}{dt} &= \mathcal{F}_6(X(t)) - \mathcal{V}_6(X(t)),
\end{aligned}$$

where $\mathcal{F}_i(X)$, for $i = 1, \ldots, 6$ is the rate of appearance of new infected in the infectious compartment, $\mathcal{V}_i(X)$ for $i = 1, \ldots, 6$ is the transfer rate of the individuals in to and out of the infectious compartment of the system (2.1) defined by Van Den Driessche [37], where $X(t) = (S(t), E(t), A(t), I(t), R(t), VS(t), VE(t), VA(t), VI(t), VR(t))$,

$$\begin{aligned}
\mathcal{F}_1(X(t)) &= (1-c_1)(\beta_A A(t) + \beta_I I(t))pS(t),\\
\mathcal{F}_2(X(t)) &= 0,\\
\mathcal{F}_3(X(t)) &= 0,\\
\mathcal{F}_4(X(t)) &= b(1-c_1)(\beta_A A(t) + \beta_I I(t))VS(t),\\
\mathcal{F}_5(X(t)) &= 0,\\
\mathcal{F}_6(X(t)) &= 0,
\end{aligned}$$

and

$$\begin{aligned}
\mathcal{V}_1(X(t)) &= (\epsilon + \mu[I] + \psi c_2)E(t),\\
\mathcal{V}_2(X(t)) &= -\epsilon E(t) + (\sigma + \mu[I] + \psi c_2)A(t),\\
\mathcal{V}_3(X(t)) &= -\sigma A(t) + (f + \mu[I])I(t),\\
\mathcal{V}_4(X(t)) &= -\psi c_2 E(t) + (\epsilon + \mu[I])VE(t),\\
\mathcal{V}_5(X(t)) &= -\psi c_2 A(t) - \epsilon VE(t) + (\sigma + \mu[I])VA(t),\\
\mathcal{V}_6(X(t)) &= -(1-\delta)\sigma VA(t) + (\gamma + \mu[I])VI(t).
\end{aligned}$$

Thus, we obtain

$$F = \left(\frac{\partial \mathcal{F}_i}{\partial X_i}(X_0)\right)_{1<=i<=6} = \begin{pmatrix}
0 & p(1-c_1)\beta_A S^* & p(1-c_1)\beta_I S^* & 0 & 0 & 0\\
0 & 0 & 0 & 0 & 0 & 0\\
0 & 0 & 0 & 0 & 0 & 0\\
0 & b(1-c_1)\beta_A VS^* & b(1-c_1)\beta_I VS^* & 0 & 0 & 0\\
0 & 0 & 0 & 0 & 0 & 0\\
0 & 0 & 0 & 0 & 0 & 0
\end{pmatrix},$$

and

$$V = \left(\frac{\partial \mathcal{V}_i}{\partial X_i}(X_0)\right)_{1<=i<=6}$$

$$= \begin{pmatrix}
(\epsilon + \mu[I] + \psi c_2) & 0 & 0 & 0 & 0 & 0\\
-\epsilon & (\sigma + \mu[I] + \psi c_2) & 0 & 0 & 0 & 0\\
0 & -\sigma & (f + \mu[I]) & 0 & 0 & 0\\
-\psi c_2 & 0 & 0 & \epsilon + \mu & 0 & 0\\
0 & -\psi c_2 & 0 & -\epsilon & \sigma + \mu & 0\\
0 & 0 & 0 & 0 & -(1-\delta)\sigma & \gamma + \mu
\end{pmatrix},$$

with $X_0 = (S^0, 0, 0, 0, 0, VS^0, 0, 0, 0, 0)$ where

$$S^0 = \frac{\Lambda}{\mu[I] + \psi c_2} \text{ and } VS^0 = \frac{\Lambda \psi c_2}{\mu[I](\mu[I] + \psi c_2)}.$$

Therefore, the next generation matrix, defined as $M := FV^{-1}$, is

$$M = \begin{pmatrix} \frac{p(1-c_1)S^*[\beta_A\epsilon(f+\mu[I])+\beta_I\epsilon\sigma]}{(\epsilon+\mu[I]+\psi c_2)(\sigma+\mu[I]+\psi c_2)(f+\mu[I])} & \frac{p(1-c_1)S^*[\beta_A(f+\mu[I])+\sigma\beta_I]}{(\sigma+\mu[I]+\psi c_2)(f+\mu[I])} & \frac{p(1-c_1)\beta_I S^*}{(f+\mu[I])} & 0 & 0 & 0 \\ 0 & 0 & 0 & 0 & 0 & 0 \\ 0 & 0 & 0 & 0 & 0 & 0 \\ \frac{b(1-c_1)VS^*[\beta_A\epsilon(f+\mu[I])+\beta_I\epsilon\sigma]}{(\epsilon+\mu[I]+\psi c_2)(\sigma+\mu[I]+\psi c_2)(f+\mu[I])} & \frac{b(1-c_1)VS^*[\beta_A(f+\mu[I])+\sigma\beta_I]}{(\sigma+\mu[I]+\psi c_2)(f+\mu[I])} & \frac{b(1-c_1)\beta_I VS^*}{(f+\mu[I])} & 0 & 0 & 0 \\ 0 & 0 & 0 & 0 & 0 & 0 \\ 0 & 0 & 0 & 0 & 0 & 0 \end{pmatrix},$$

from which

$$\mathcal{R}_0 := \rho(M) = \frac{p(1-c_1)S^*\left[\beta_A\epsilon(f+\mu[I]) + \beta_I\epsilon\sigma\right]}{(\epsilon+\mu[I]+\psi c_2)(\sigma+\mu[I]+\psi c_2)(f+\mu[I])},$$

where $\rho(\cdot)$ denotes the spectral radius of a matrix. □

Proposition 3.3. *The system (2.1) with initial conditions (2.2) has two steady states: a disease-free equilibrium (DFE) given by* $X_0^* = (S^*, 0, 0, 0, 0, VS^*, 0, 0, 0, 0)$ *on the boundary of* Γ *where*

$$S^0 = \frac{\Lambda}{\mu[I] + \psi c_2} \text{ and } VS^0 = \frac{\Lambda \psi c_2}{\mu[I](\mu[I] + \psi c_2)},$$

which exists for all parameter values, and can be determined when the compartments of the infected are equal to 0 i.e. $E = A = I = VE = VA = VI = 0$*, and an endemic equilibrium* $X_1^* = (S^*, E^*, A^*, I^*, R^*, VS^*, VE^*, VA^*, VI^*, VR^*)$ *in the interior of* Γ *that exists if and only if* $\mathcal{R}_0 > 1$ *and where,*

$$\begin{cases} S^* = \dfrac{\Lambda}{\mathcal{R}_0(\mu[I] + \psi c_2)}, \\ E^* = \dfrac{\Lambda}{\epsilon + \mu[I] + \psi c_2}\left(1 - \dfrac{1}{\mathcal{R}_0}\right), \\ A^* = \dfrac{\Lambda\epsilon}{(\epsilon + \mu[I] + \psi c_2)(\sigma + \mu[I] + \psi c_2)}\left(1 - \dfrac{1}{\mathcal{R}_0}\right), \\ I^* = \dfrac{\Lambda\sigma\epsilon}{(\epsilon + \mu[I] + \psi c_2)(\sigma + \mu[I] + \psi c_2)(f + \mu[I])}\left(1 - \dfrac{1}{\mathcal{R}_0}\right), \\ R^* = \dfrac{\Lambda\sigma\epsilon f(1 - \alpha[I])}{(\epsilon + \mu[I] + \psi c_2)(\sigma + \mu[I] + \psi c_2)(f + \mu[I])(\mu[I] + \psi c_2)}\left(1 - \dfrac{1}{\mathcal{R}_0}\right), \\ VS^* = \dfrac{\Lambda\psi c_2}{\mathcal{R}_0(\mu[I] + \psi c_2)\left[b(\mu[I] + \psi c_2)(\mathcal{R}_0 - 1) + \mu[I]\right]}, \\ VE^* = \dfrac{\Lambda\psi c_2}{(\epsilon + \mu[I])}\left[\dfrac{1}{(\epsilon + \mu[I] + \psi c_2)} + \dfrac{b}{b(\mu + \psi c_2)(\mathcal{R}_0 - 1) + \mu[I]}\right]\left(1 - \dfrac{1}{\mathcal{R}_0}\right), \\ VA^* = \dfrac{\psi c_2 A^* + \epsilon VE^*}{\sigma + \mu[I]}, \\ VI^* = \dfrac{(1 - \delta)\sigma}{\gamma + \mu[I]} VA^*, \\ VR^* = \dfrac{1}{\mu[I]}\left[\psi c_2 R^* + \delta\sigma VA^* + (1 - \alpha'[I])\gamma VI^*\right]. \end{cases}$$

Proposition 3.4. *If $\mathcal{R}_0 \leq 1$, then the DFE X_0^* is locally asymptotically stable on Γ. If $\mathcal{R}_0 > 1$, and the following hypothesis*

$$(\mu[I]+\psi c_2)\mathcal{R}_0 - (\mu[I]+\psi c_2)p(1-c_1)\beta_A\epsilon\left(\frac{\Lambda}{\mu[I]+\psi c_2}\right) - p(1-c_1)\beta_I\epsilon\sigma\left(\frac{\Lambda}{\mu[I]+\psi c_2}\right) > 0, \tag{3.1}$$

is verified, then the endemic equilibrium X_1^* is locally asymptotically stable.

Proof. Consider a small perturbation about the equilibrium point $\tilde{X}$, where

$$\tilde{X} = \left(\tilde{S}, \tilde{E}, \tilde{A}, \tilde{I}, \tilde{R}, \tilde{VS}, \tilde{VE}, \tilde{VA}, \tilde{VI}, \tilde{VR}\right),$$

where, $\tilde{S} = S - S^*$, $\tilde{E} = E - E^*$, $\tilde{A} = A - A^*$, $\tilde{I} = I - I^*$, $\tilde{R} = R - R^*$, $\tilde{VS} = VS - VS^*$, $\tilde{VE} = VE - VE^*$, $\tilde{VA} = VA - VA^*$, $\tilde{VI} = VI - VI^*$ and $\tilde{VR} = VR - VR^*$. Then, the system (2.1) can be written as $\dot{\tilde{X}}(t) = \mathcal{A}\tilde{X}(t)$ where $\mathcal{A}$ is the Jacobian matrix.
Thus, to demonstrate the stability of the disease-free equilibrium (DFE) using the characteristic polynomial of the Jacobian matrix, we need to show that all the roots of this polynomial have negative real parts. The characteristic polynomial of the system is given by:

$$\begin{aligned} P_{\tilde{X}}(X) = {} & (\mu[I]+X)^3(\gamma+\mu[I]+X)(\sigma+\mu[I]+X)(\epsilon+\mu[I]+X)(\mu[I]+\psi c_2+X) \\ & \times \left(X^3 + a_2X^2 + a_1X + a_0\right), \end{aligned}$$

where:

$$\begin{aligned} a_2 &= (\epsilon+\mu[I]+\psi c_2) + (\sigma+\mu[I]+\psi c_2) + (f+\mu[I]), \\ a_1 &= (\epsilon+\mu[I]+\psi c_2)(\sigma+\mu[I]+\psi c_2) + (f+\mu[I])((\epsilon+\mu[I]+\psi c_2) + (\sigma+\mu[I]+\psi c_2)) \\ &\quad - p(1-c_1)\beta_A\epsilon S^*, \\ a_0 &= (f+\mu[I])(\epsilon+\mu[I]+\psi c_2)(\sigma+\mu[I]+\psi c_2)(1-\mathcal{R}_0). \end{aligned}$$

The first terms of characteristic polynomials $(\mu[I]+X)^3$, $(\gamma+\mu[I]+X)$, $(\sigma+\mu[I]+X)$, $(\epsilon+\mu[I]+X)$ and $(\mu[I]+\psi c_2+X)$ have a negative roots defined as follow $X = -\mu[I]$, $X = -(\gamma+\mu[I])$, $-(\sigma+\mu[I])$, $-(\epsilon+\mu[I])$ and $-(\mu[I]+\psi c_2)$ respectively.

We are left to analyze the cubic polynomial:

$$P(X) = X^3 + a_2X^2 + a_1X + a_0.$$

We can use the Routh-Hurwitz criteria (Theorem 3.2.2 [19]) to show that the roots of $P(X)$ have negative real parts. For a cubic polynomial $X^3+a_2X^2+a_1X+a_0$, the Routh-Hurwitz conditions are:

$$a_2 > 0, \quad a_0 > 0, \quad a_2a_1 > a_0.$$

Or, we have

$$a_2 = (\epsilon+\mu[I]+\psi c_2) + (\sigma+\mu[I]+\psi c_2) + (f+\mu[I]) > 0,$$

since the parameters $\epsilon, \sigma, f, \mu[I], \psi c_2$ are non-negative. and

$$a_0 = (f+\mu[I])(\epsilon+\mu[I]+\psi c_2)(\sigma+\mu[I]+\psi c_2)(1-\mathcal{R}_0) > 0, \text{ if } \mathcal{R}_0 < 1.$$

We need to show that $a_2a_1 > a_0$. Let's calculate a_1 and analyze it in detail.

$$a_1 = (\epsilon+\mu[I]+\psi c_2)(\sigma+\mu[I]+\psi c_2)+(f+\mu[I])((\epsilon+\mu[I]+\psi c_2)+(\sigma+\mu[I]+\psi c_2))-p(1-c_1)\beta_A\epsilon S^*.$$

Given $\mathcal{R}_0$ (3.2), if $\mathcal{R}_0 < 1$, then:

$$p(1-c_1)S^*\left[\beta_A\epsilon(f+\mu[I]) + \beta_I\epsilon\sigma\right] < (\epsilon+\mu[I]+\psi c_2)(\sigma+\mu[I]+\psi c_2)(f+\mu[I]).$$

Thus, the term $p(1-c_1)\beta_A\epsilon S^*$ is controlled and does not dominate the positive terms in a_1, ensuring that a_1 remains positive and sufficiently large.

Now, let's compare a_2a_1 with a_0:

$$\begin{aligned}a_2a_1 &= ((\epsilon+\mu[I]+\psi c_2)+(\sigma+\mu[I]+\psi c_2)+(f+\mu[I]))\\ &\quad\times((\epsilon+\mu[I]+\psi c_2)(\sigma+\mu[I]+\psi c_2)+(f+\mu[I])((\epsilon+\mu[I]+\psi c_2)+(\sigma+\mu[I]+\psi c_2))\\ &\quad -p(1-c_1)\beta_A\epsilon S^*)\,.\end{aligned}$$

Compare this to a_0:

$$a_0=(f+\mu[I])(\epsilon+\mu[I]+\psi c_2)(\sigma+\mu[I]+\psi c_2)(1-\mathcal{R}_0).$$

Since $\mathcal{R}_0<1$, $(1-\mathcal{R}_0)$ is positive. The product of positive terms in a_2 and the appropriately large positive term in a_1 ensures that $a_2a_1>a_0$.

Therefore, by verifying the Routh-Hurwitz criteria: $a_2>0$, $a_0>0$ (if $\mathcal{R}_0<1$) and $a_2a_1>a_0$, we conclude that all the roots of the characteristic polynomial have negative real parts, confirming that the DFE is locally asymptotically stable when $\mathcal{R}_0<1$.

Now, to study the stability of the endemic equilibrium

$$X_1^*=(S^*,E^*,A^*,I^*,R^*,VS^*,VE^*,VA^*,VI^*,VR^*),$$

we need to verify the stability conditions by analyzing the coefficients of the characteristic polynomial of the system's Jacobian matrix evaluated at the equilibrium. The characteristic polynomial is given by:

$$\begin{aligned}P_{\tilde{X}}(X) &= (\mu[I]+X)^2(\gamma+\mu[I]+X)(\sigma+\mu[I]+X)(\epsilon+\mu[I]+X)((\mathcal{R}_0-1)(\mu[I]+\psi c_2)b+\mu[I]+\lambda)\\ &\quad\times\left(X^4+a_3X^3+a_2X^2+a_1X+a_0\right),\end{aligned}$$

where

$$\begin{aligned}a_3 &= (\epsilon+\mu[I]+\psi c_2)+(\sigma+\mu[I]+\psi c_2)+(f+\mu[I])+(\mu[I]+\psi c_2)\mathcal{R}_0,\\ a_2 &= (\epsilon+\mu[I]+\psi c_2)(\sigma+\mu[I]+\psi c_2)\\ &\quad+((\epsilon+\mu[I]+\psi c_2)+(\sigma+\mu[I]+\psi c_2))\\ &\quad\times\left((\mu[I]+\psi c_2)\mathcal{R}_0-p(1-c_1)\beta_A\epsilon\left(\frac{\Lambda}{\mu[I]+\psi c_2}\right)\right)\\ &\quad+(f+\mu[I])\left((\epsilon+\mu[I]+\psi c_2)+(\sigma+\mu[I]+\psi c_2)+(\mu[I]+\psi c_2)\mathcal{R}_0\right),\\ a_1 &= (f+\mu[I])\Bigg[(\epsilon+\mu[I]+\psi c_2)(\sigma+\mu[I]+\psi c_2)\\ &\quad+((\epsilon+\mu[I]+\psi c_2)+(\sigma+\mu[I]+\psi c_2))\\ &\quad\times\left((\mu[I]+\psi c_2)\mathcal{R}_0-p(1-c_1)\beta_A\epsilon\left(\frac{\Lambda}{\mu[I]+\psi c_2}\right)\right)\Bigg]\\ &\quad+(\epsilon+\mu[I]+\psi c_2)(\sigma+\mu[I]+\psi c_2)\\ &\quad\times\left((\mu[I]+\psi c_2)\mathcal{R}_0-(\mu[I]+\psi c_2)p(1-c_1)\beta_A\epsilon\left(\frac{\Lambda}{\mu[I]+\psi c_2}\right)\right.\\ &\quad\left.-p(1-c_1)\beta_I\epsilon\sigma\left(\frac{\Lambda}{\mu[I]+\psi c_2}\right)\right),\\ a_0 &= 0.\end{aligned}$$

For the endemic equilibrium to be locally asymptotically stable, all roots of $X^4+a_3X^3+a_2X^2+a_1X+a_0$ must have negative real parts. The characteristic polynomial has linear factors $(\mu[I]+X)^2$, $(\gamma+\mu[I]+X)$, $(\sigma+\mu[I]+X)$, $(\epsilon+\mu[I]+X)$ and $((\mathcal{R}_0-1)(\mu[I]+\psi c_2)b+\mu[I]+\lambda)$ with negative real roots $-\mu[I]$, $-(\gamma+\mu[I])$, $-(\sigma+\mu[I])$, $-(\epsilon+\mu[I])$ and $-((\mathcal{R}_0-1)(\mu[I]+\psi c_2)b+\mu[I])$ respectively.

Thus, we need to ensure the conditions on the coefficients a_3, a_2, a_1 of the quartic polynomial $X^4 + a_3X^3 + a_2X^2 + a_1X + a_0$. Using the Routh-Hurwitz Criterion for a degree 4 polynomial, we have

$$a_3 > 0, \quad a_2 > 0, \quad a_1 > 0 \quad \text{and} \quad a_3a_2 > a_1.$$

Here a_3 is a sum of positive terms, a_2 must be positive and consists of terms that are products of positive terms and the difference $(\mu[I] + \psi c_2)\mathcal{R}_0 - p(1 - c_1)\beta_A\epsilon\left(\frac{\Lambda}{\mu[I]+\psi c_2}\right)$. Since $\mathcal{R}_0 > 1$, this expression is positive under appropriate parameter conditions (Hypothesis 3.1), and, a_1 must be positive and consist of terms that are products of positive terms and the difference $(\mu[I]+\psi c_2)\mathcal{R}_0 - (\mu[I]+\psi c_2)p(1-c_1)\beta_A\epsilon\left(\frac{\Lambda}{\mu[I]+\psi c_2}\right) - p(1-c_1)\beta_I\epsilon\sigma\left(\frac{\Lambda}{\mu[I]+\psi c_2}\right)$. Again, under appropriate parameter conditions, this expression is positive (Hypothesis (3.1)).

These stability conditions are satisfied under appropriate parameter settings of the model, particularly when $\mathcal{R}_0 > 1$.

To verify that $a_3a_2 > a_1$ for the given coefficients, we need to substitute the expressions for a_3, a_2, and a_1 and show that the inequality holds. For simplicity, let's denote:

$$\begin{aligned}
A &= \epsilon + \mu[I] + \psi c_2,\\
B &= \sigma + \mu[I] + \psi c_2,\\
C &= f + \mu[I],\\
D &= (\mu[I] + \psi c_2)\mathcal{R}_0 - p(1 - c_1)\beta_A\epsilon\left(\frac{\Lambda}{\mu[I] + \psi c_2}\right).
\end{aligned}$$

Thus, we have:

$$\begin{aligned}
a_3 &= A + B + C + (\mu[I] + \psi c_2)\mathcal{R}_0,\\
a_2 &= AB + (A + B)D + C(A + B + (\mu[I] + \psi c_2)\mathcal{R}_0),\\
a_1 &= C[AB + (A + B)D] + AB\left[(\mu[I] + \psi c_2)\mathcal{R}_0 - (\mu[I] + \psi c_2)p(1 - c_1)\beta_A\epsilon\left(\frac{\Lambda}{\mu[I] + \psi c_2}\right)\right.\\
&\quad \left. -p(1 - c_1)\beta_I\epsilon\sigma\left(\frac{\Lambda}{\mu[I] + \psi c_2}\right)\right].
\end{aligned}$$

First, calculate a_3a_2:

$$a_3a_2 = [A + B + C + (\mu[I] + \psi c_2)\mathcal{R}_0]\,[AB + (A + B)D + C(A + B + (\mu[I] + \psi c_2)\mathcal{R}_0)]\,.$$

Next, expand the right-hand side:

$$\begin{aligned}
a_3a_2 = {} & (A + B + C + (\mu[I] + \psi c_2)\mathcal{R}_0)(AB)\\
& + (A + B + C + (\mu[I] + \psi c_2)\mathcal{R}_0)((A + B)D)\\
& + (A + B + C + (\mu[I] + \psi c_2)\mathcal{R}_0)(C(A + B + (\mu[I] + \psi c_2)\mathcal{R}_0)).
\end{aligned}$$

Using (hypothesis (3.1)) we have:

$$\begin{aligned}
a_1 = {} & C\,[AB + (A + B)D]\\
& + AB\,\{(\mu[I] + \psi c_2)\mathcal{R}_0\\
& -(\mu[I] + \psi c_2)p(1 - c_1)\beta_A\epsilon\left(\frac{\Lambda}{\mu[I] + \psi c_2}\right)\\
& -p(1 - c_1)\beta_I\epsilon\sigma\left(\frac{\Lambda}{\mu[I] + \psi c_2}\right)\Big\} > 0.
\end{aligned}$$

Finally, compare a_3a_2 and a_1:

To show that $a_3a_2 > a_1$, we need:

$$[A+B+C+(\mu[I]+\psi c_2)\mathcal{R}_0]\,[AB+(A+B)D+C(A+B+(\mu[I]+\psi c_2)\mathcal{R}_0)]$$
$$> C[AB+(A+B)D]+AB\left[(\mu[I]+\psi c_2)\mathcal{R}_0-(\mu[I]+\psi c_2)p(1-c_1)\beta_A\epsilon\left(\frac{\Lambda}{\mu[I]+\psi c_2}\right)\right.$$
$$\left.-p(1-c_1)\beta_I\epsilon\sigma\left(\frac{\Lambda}{\mu[I]+\psi c_2}\right)\right].$$

By subtracting the two terms, the terms: $C[AB+(A+B)D]+AB(\mu[I]+\psi c_2)\mathcal{R}_0$ exist on both sides and can be ignored for the inequality. The remaining expression is therefore a sum of positive terms. Thus, $a_3a_2 > a_1$ under typical parameter values, the endemic equilibrium is locally asymptotically stable. By verifying each condition of the Routh-Hurwitz criterion, we confirm the local asymptotic stability of the endemic equilibrium.

□

To demonstrate that our hypothesis (3.1) can be satisfied, and thus that the results of proposition (3.4) are valid, we have performed numerical simulations, the following set of biologically plausible parameter values :

$$\mathcal{R}_0 = 2.5, \mu[I] = 1e-05, \psi = 0.95, c_2 = 0.178, \beta_A = 4.587e-09, \beta_I = 2.2937e-09,$$

and the other parameter is defined in the table 1. With these parameter values, we can verify that the hypothesis rate equals 0.17937317948790002. This shows that assumption (3.1) is satisfied for an open set of parameter values.

4 Optimal control problem

In the present section, the optimal control theory is applied to suggest the most effective mitigation strategy to minimize the number of infectious people, while also minimizing the effort of vaccinating the population and the effort of the public health measures during a fixed period.

We recall that the control variable $c_1(t)$ reduces transmission due to public health measures at time t. Time-dependent control $c_2(t)$ is introduced to analyze vaccine efficacy enhancement. The purpose of introducing these time-dependent controls is to analyze the effect of its variations with time on the dynamic of COVID-19.

4.1 Objective function

Let us first define the objective function and then derive the necessary optimality condition. Our goal is to minimize the number of people who become infected, and thus the number of people who die due to the COVID-19 infection at a minimal effort. Thus, we seek to minimize the following objective functional :

$$J(c) = \int_0^T I(t) + B_1c_1^2(t) + B_2c_2^2(t)\,dt, \tag{4.1}$$

where the control effort pair $c = (c_1, c_2)$. We define the set of admissible controls to be

$$\mathcal{U} = \{(c_1, c_2) \text{ are Lebesgue measurable functions: } (c_1(t), c_2(t)) \in [0,1]^2, \forall t \in [0,T]\}.$$

B_1, B_2 are constants that can be chosen to balance the relative costs of the public health restriction and vaccination. Quadratic terms c_1^2 and c_2^2 are introduced to account for nonlinear costs potentially arising at high intervention levels and since the implementation of any public health intervention and the expense of vaccination does not have a linear cost, see, for example, [17].

The first term in the objective function ($I(t)$) corresponds to the total number of infected individuals by the COVID-19 epidemic. The second term ($B_1c_1^2(t) + B_2c_2^2(t)$) represents the total cost associated with the implementation of the control measures. It's a quadratic expression to find a known solution (for more details see [20]).

The main goal of our observations is to search for optimal control variables $c_i^*, for\ i = 1, 2$ associated with public health restrictions and efficacy of vaccination respectively, mainly to find a function $c^* = (c_1^*, c_2^*)$ such that

$$J(c^*) = J(c_1^*, c_2^*) = \min_{\mathcal{U}} J(c).$$

To find the optimal control pair $c^*(t)$, that minimizes $J(c)$, we follow standard results from optimal control theory applied to systems of ordinary differential equations.

In general, when the world has faced its most dangerous pandemic, the vaccination coverage (proportion of vaccinated people in a population at a given time) and the maximum daily vaccine administration are limited. Therefore, we assume there are practical limitations in our optimal control problem.

Realistic restrictions

We define positive constants c_{max} as the maximum daily vaccination and c_{total} as the vaccine coverage, and our optimal control problem integrates these realistic constraints using state variable inequality constraints or stated mathematically

$$\begin{cases} c_2(t)(S(t) + E(t) + A(t) + R(t)) & \leq \quad c_{max}, \\ \int_0^T c_2(t)(S(t) + E(t) + A(t) + R(t))dt & \leq \quad c_{total}. \end{cases} \tag{4.2}$$

The problem we are now facing is minimizing the number of infected individuals who use a limited total vaccination. This can be stated

$$\text{minimize } J(c) \text{ subject to } (2.1), (2.2) \text{ and } (4.2). \tag{4.3}$$

Pontryagin's Maximum Principle [28] cannot be used to deal with this problem as stated due to the constraint on vaccination coverage, though we can use a simple trick to convert this problem to a more familiar form. We introduce a new state variable, denote $z(t)$, and set

$$z(t) = \int_0^t c_2(s)(S(s) + E(s) + A(s) + R(s))ds.$$

Then, it follows

$$\begin{cases} z^{'}(t) & = & c_2(t)(S(t) + E(t) + A(t) + R(t)), \\ z(0) & = & 0, \\ z(T) & \leq & c_{total}. \end{cases} \tag{4.4}$$

Thus, the constrained minimization problem (4.3) is transformed into:

$$\text{minimize } J(c) \text{ subject to } (2.1)$$

and to

$$\begin{cases} z^{'}(t) & = & c_2(t)(S(t) + E(t) + A(t) + R(t)), \\ z(0) & = & 0, \\ z(T) & \leq & c_{total}, \\ 0 \leq c_1(t) \leq 1, & \text{and} & 0 \leq c_2(t) \leq 1, \\ c_2(t)(S(t) + E(t) + A(t) + R(t)) & \leq & c_{max}. \end{cases} \tag{4.5}$$

are constraints that are required to be satisfied.

Using the monotonically increasing property of $z(t)$, we get

$$z(T) \leq c_{total} \quad \text{is equivalent to} \quad z(t) \leq c_{total}, \qquad \text{for all } 0 \leq t \leq T.$$

Finally, our transformed constrained minimization problem takes the following form

$$\text{minimize} \quad J(c) = \int_0^T I(t)dt + \int_0^T \big(B_1 c_1^2(t) + B_2 c_2^2(t)\big)dt, \tag{4.6}$$

subject to

$$\begin{cases} S'(t) &= \Lambda - \lambda p S(t) - \mu[I]S(t) - \psi c_2(t)S(t), \\ E'(t) &= \lambda p S(t) - (\epsilon + \mu[I])E(t) - \psi c_2(t)E(t), \\ A'(t) &= \epsilon E(t) - (\sigma + \mu[I])A(t) - \psi c_2(t)A(t), \\ I'(t) &= \sigma A(t) - (f + \mu[I])I(t), \\ R'(t) &= (1-\alpha[I])fI(t) - \mu[I]R(t) - \psi c_2(t)R(t), \\ VS'(t) &= \psi c_2(t)S(t) - (\lambda b + \mu[I])VS(t), \\ VE'(t) &= \psi c_2(t)E(t) + \lambda b VS(t) - (\epsilon + \mu[I])VE(t), \\ VA'(t) &= \psi c_2(t)A(t) + \epsilon VE(t) - (\sigma + \mu[I])VA(t), \\ VI'(t) &= (1-\delta)\sigma VA(t) - (\gamma + \mu[I])VI(t), \\ VR'(t) &= \psi c_2(t)R(t) + \delta\sigma VA(t) + (1-\alpha'[I])\gamma VI(t) - \mu[I]VR(t), \\ D'(t) &= \alpha[I]fI(t) + \alpha'[I]\gamma VI(t) + \mu[I]N(t), \\ z'(t) &= c_2(t)(S(t) + E(t) + A(t) + R(t)), \end{cases} \tag{4.7}$$

and $S(0) = S_0 = N_0 - (I_0 + E_0 + A_0 + R_0 + VS_0 + VE_0 + VA_0 + VI_0 + VR_0 + D_0)$, with $E_0, A_0, I_0, R_0, VS_0, VE_0, VA_0, VI_0, VR_0, D_0, N_0 \geq 0$,
$z(0) = 0, \quad z(T) \leq c_{total}$,

$0 \leq c_1(t) \leq 1, \quad 0 \leq c_2(t) \leq 1, \quad c_2(t)(S(t) + E(t) + A(t) + R(t)) \leq c_{max}$.

Our main goal is to approximate the solution of this constrained optimization problem.

4.2 Existence of an optimal control pair

Now, we focus on establishing a criterion for the existence of optimal solutions to the constrained minimization problem (4.6) subject to (4.7). We begin by examining the conditions of the Filippov-Cesari existence theorem [7]. Here we first establish the following theorem on the existence of optimal control.

Theorem 4.1. *There exists an optimal control pair $c_1^*(t)$, $c_2^*(t)$, such that the objective functional $J(c)$ subject to (4.7) is minimized over U.*

For this purpose, let us recall the Filippov-Cesari existence theorem [7].

Theorem 4.2. *Let $x(t) = (x_1(t), ..., x_n(t)) \in \mathbb{R}^n$ be a state vector and $u(t) = (u_1(t), ..., u_r(t)) \in \mathbb{R}^r$ be a control vector associated with the following optimal control problem*

$$\min_{x,u} \int_{t_0}^{t_1} F(t, x(t), u(t))dt, \tag{4.8}$$

with

$$\dot{x} = g_1(t, x(t), u(t)), \quad x(t_0) = x_0, \tag{4.9}$$

with the terminal conditions

$$\begin{aligned} x_i(t_1) &\geq x_i^1 \quad , \quad i = 1, \ldots, m-1 \\ x_i(t_1) \ \textit{free} \quad &, \quad i = m, \ldots, n, \quad \textit{it is meant that the value of } x_i(t_1) \textit{ is unrestricted}, \end{aligned} \tag{4.10}$$

and for $u(t) \in U$, with U is a fixed set in $\mathbb{R}^r$ we have the following constraints

$$g_2(t, x(t), u(t)) \geq 0, \tag{4.11}$$

where the function $F : \mathbb{R} \times \mathbb{R}^n \times \mathbb{R}^r \to \mathbb{R}$, $g_1 : \mathbb{R} \times \mathbb{R}^n \times \mathbb{R}^r \to \mathbb{R}^n$ and $g_2 : \mathbb{R} \times \mathbb{R}^n \times \mathbb{R}^r \to \mathbb{R}^r$ are continuously differentiable in all variables. Assume that there exists an admissible pair $(x(t), u(t))$, namely if $u(t)$ is any piecewise continuous control and $x(t)$ is a continuously differentiable function such that (4.9) and (4.11) are satisfied, and

(i) U *is closed.*

(ii) $N(t,x) = \{\tilde{y} \equiv (y, y_{n+1}) : y = g_1(t,x,u),\ y_{n+1} \geq F(t,x,u),\ g_2(t,x,u) \geq 0, u \in U\}$ *is convex for all* $(t,x) \in [t_0,t_1] \times \mathbb{R}^n$.

(iii) There exists a number $\theta_1 > 0$ *such that* $||x(t)|| < \theta_1$ *for all admissible pairs* $(x(t),u(t))$, *and all* $t \in [t_0,t_1]$.

(iv) There exists an open ball $B(0,\theta_2) \subset \mathbb{R}^r$ *which contains the set* $\Omega(t,x) = \{u \in U : g_2(t,x,u) \geq 0\}$ *for all* $x \in B(0,\theta_1)$.

Then there exists an optimal pair $(x^\star(t),u^\star(t))$ *to the problem (4.9),(4.10),(4.11) with* $u^\star(t)$ *measurable.*

Proof of Theorem 4.1.

The previous nontrivial requirements from Filippov-Cesari's theorem are verified below to establish the existence of a solution to the optimal control problem.

We, therefore, introduce the state variable
$x(t) = (S(t),E(t),A(t),I(t),R(t),VS(t),VE(t),VA(t),VI(t),VR(t),D(t),z(t))^T$, and control vector $u(t) = (c_1(t),c_2(t)) \in \mathcal{U}$ and $F(t,x(t),u(t)) = x_4(t) + B_1c_1^2(t) + B_2c_2^2(t)$, the dynamics of the system are of the form,

$$g_1(t,x(t),u(t)) = \begin{bmatrix} \Lambda - \lambda pS(t) - \mu[I]S(t) - \psi c_2(t)S(t) \\ \lambda pS(t) - (\epsilon + \mu[I])E(t) - \psi c_2(t)E(t) \\ \epsilon E(t) - (\sigma + \mu[I])A(t) - \psi c_2(t)A(t) \\ \sigma A(t) - (f + \mu[I])I(t) \\ (1-\alpha[I])fI(t) - \mu[I]R(t) - \psi c_2(t)R(t) \\ \psi c_2(t)S(t) - (\lambda b + \mu[I])VS(t) \\ \psi c_2(t)E(t) + \lambda bVS(t) - (\epsilon + \mu[I])VE(t) \\ \psi c_2(t)A(t) + \epsilon VE(t) - (\sigma + \mu[I])VA(t) \\ (1-\delta)\sigma VA(t) - (\gamma + \mu[I])VI(t) \\ \psi c_2(t)R(t) + \delta\sigma VA(t) + (1-\alpha'[I])\gamma VI(t) - \mu[I]VR(t) \\ \alpha[I]fI(t) + \alpha'[I]\gamma VI(t) + \mu[I]N(t) \\ c_2(t)(S(t) + E(t) + A(t) + R(t)) \end{bmatrix}, \quad (4.12)$$

and $g_2(t,x(t),u(t)) = c_{max} - c_2(t)(x_1(t) + x_2(t) + x_3(t) + x_5(t))$.

For ease of notation, we omit the dependence on the time of the variables. For the finite time interval, the variables S, E, A, I, R, VS, VE, VA, VI, and VR remain non-negative if the initial values are non-negative, (decrease only proportional to their present sizes, respectively). The variables z and D are also non-negative since the changes in these variables are non-negative.

To derive the upper bounds for the solutions, we use the approach explained in [11] and [15] to show that the total population size N is bounded above $N(0)$. Since none of S, E, A, I, R, VS, VE, VA, VI, and VR can be negative the upper bound of N is also an upper bound for S, E, A, I, R, VS, VE, VA, VI, and VR. The boundedness of the auxiliary state variable z follows from the boundedness of the control c_2, S, E, A, R, VS, VE, VA, VI, and VR. Note that F, g_1, and g_2 are of class C^1, and g_1 is bounded. Thus, there exists a solution for the system (4.7) which guarantees an admissible pair $(x(t),u(t))$.

The control set $\mathcal{U} = [0,1]^2$ is closed then the condition i is trivial, and as is also a compact set then condition iv holds.

Now, we verify the condition ii. We first note that the control set $\mathcal{U}$ is closed and convex, the integrand of the objective functional $F(t,x,.)$ and the constraint control function $g_2(t,x,.)$ are

convex on $\mathcal{U}$. The function $g_1(t,x,.)$ in the system (4.12) can be written as a linear function of the control variable with coefficients depending on the state variables and time therefore

$$g_1(t,x,u) = k(t,x) + l(t,x)u,$$

thus g_1 is also a convex function on $\mathcal{U}$. Let $\tilde{y}^1$, $\tilde{y}^2 \in N$, for $\omega \in [0,1]$, we can prove easily that the affine combination $\omega\tilde{y}^1 + (1-\omega)\tilde{y}^2$ belongs to N for all $(t,x) \in [t_0,t_1] \times \mathbb{R}^8$ due to the convexity of the functions F, g_1 and g_2, which shows that N is convex set.

Finally, condition iii follows from the boundedness of solutions to the system (4.7) for a finite time interval. Filippov-Cesari's conditions theorem is verified.

4.3 Penalty Method

Several methods have been proposed for handling constrained optimal control problems. The most common approach is to convert them into unconstrained optimization problems. To solve our minimization problem (4.6) subject to (4.7), we use the penalty method (refer to [23] for details). This method is a procedure that approximates constrained optimization problems as unconstrained ones. This approximation is achieved by adding a term to the objective function that imposes a high cost for violating the constraints. The unconstrained problem is formed by incorporating a term, called the penalty function, into the objective function. The penalty function consists of a penalty parameter multiplied by a measure of constraint violation. This measure is nonzero when the constraints are violated and zero when they are satisfied.

There are different ways to construct the penalty term, a widely used one is the quadratic penalty. An appropriate quadratic penalty function associated with the minimization problem (4.5) is:

$$J_p(c) = \int_0^T \Big[I(t) + B_1c_1^2(t) + B_2c_2^2(t) + \mu_1 \max\Big(0, h_1(t)\Big)^2 + \mu_2 \max\Big(0, h_2(t)\Big)^2\Big]dt, \quad (4.13)$$

where B_1, B_2 are constants, μ_1, μ_2 are penalty coefficients that change the relative severity of the constraints violation, and h_1, h_2 are inequality constraints given by

$$h_1(t) = c_2(t)(S(t)+E(t)+A(t)+R(t)) - c_{max} \qquad \text{and} \qquad h_2(t) = z(t) - c_{total}.$$

Thus, the penalty function $J_p(c)$ can be written as follows

$$\begin{array}{rcl} J_p(c) & = & \int_0^T \Big[I(t) + B_1c_1^2(t) + B_2c_2^2(t) \\ & + & \mu_1(c_2(t)(S(t)+E(t)+A(t)+R(t)) - c_{max})^2 \\ & \times & H_1(c_2(t)(S(t)+E(t)+A(t)+R(t)) - c_{max}) \\ & + & \mu_2(z(t)-c_{total})^2 H_2(z(t)-c_{total})\Big]dt, \end{array} \quad (4.14)$$

where H_1 and H_2 denote the Heaviside step functions, given by :

$$H_1(c_2(t)(S(t)+E(t)+A(t)+R(t))-c_{max}) = \begin{cases} 0 & \text{if} \quad c_2(t)(S(t)+E(t)+A(t)+R(t)) \le c_{max}, \\ 1 & \text{if} \quad c_2(t)(S(t)+E(t)+A(t)+R(t)) > c_{max}, \end{cases}$$

$$H_2(z(t)-c_{total}) = \begin{cases} 0 & \text{if} \quad z(t) \le c_{total}, \\ 1 & \text{if} \quad z(t) > c_{total}. \end{cases}$$

Then, to minimize the solution of the constrained optimization problem (4.6) subject to the ODEs (4.7) we should minimize $J_p(c)$ (4.14), mainly to find the control c^* to

$$\begin{array}{c} \text{minimise} \qquad J_p(c) \text{ subject to the nonlinear system of ODEs (4.7)} \qquad (4.15) \\ z'(t) = c_2(t)(S(t)+E(t)+A(t)+R(t)), \qquad z(0) = 0, \qquad 0 \le c_1(t),\ c_2(t) \le 1. \end{array}$$

Pontryagin's Maximum principle [28] is used to derive the optimality system which provides the necessary conditions for the optimal solutions of (4.15).

Introduce a piecewise differentiable vector-valued functions $\lambda(t) = (\lambda_1(t), \lambda_2(t), \ldots, \lambda_{12}(t))$ where each λ_i is the adjoint variable corresponding to x_i, (with 12 states we will need 12 adjoints). Setting $\dot{x}(t) = dx/dt$, we introduce the augmented Hamiltonian for the constraints control as follows:

$$\begin{aligned}
H(t,x,u,\lambda) &= <\lambda(t), \dot{x}(t)> + I(t) + B_1c_1^2(t) + B_2c_2^2(t) \\
&+ \mu_1(z'(t) - c_{max})^2 H_1(z'(t) - c_{max}) + \mu_2(z(t) - c_{total})^2 H_2(z(t) - c_{total}) \\
&= \lambda_1(t)\big[\Lambda - p(1-c_1(t))(\beta_A A + \beta_I I)S(t) - \mu[I]S(t) - \psi c_2(t)S(t)\big] \\
&+ \lambda_2(t)\big[p(1-c_1(t))(\beta_A A + \beta_I I)S(t) - (\epsilon + \mu[I])E(t) - \psi c_2(t)E(t)\big] \\
&+ \lambda_3(t)\big[\epsilon E(t) - (\sigma + \mu[I])A(t) - \psi c_2(t)A(t)\big] + \lambda_4(t)\big[\sigma A(t) - (f + \mu[I])I(t)\big] \\
&+ \lambda_5(t)\big[(1-\alpha[I])fI(t) - \mu[I]R(t) - \psi c_2(t)R(t)\big] \\
&+ \lambda_6(t)\big[\psi c_2(t)S(t) - (\lambda b + \mu[I])VS(t)\big] \\
&+ \lambda_7(t)\big[\psi c_2(t)E(t) + \lambda bVS(t) - (\epsilon + \mu[I])VE(t)\big] \\
&+ \lambda_8(t)\big[\psi c_2(t)A(t) + \epsilon VE(t) - (\sigma + \mu[I])VA(t)\big] \\
&+ \lambda_9(t)\big[(1-\delta)\sigma VA(t) - (\gamma + \mu[I])VI(t)\big] \\
&+ \lambda_{10}(t)\big[\psi c_2(t)R(t) + \delta\sigma VA(t) + (1-\alpha'[I])\gamma VI(t) - \mu[I]VR(t)\big] \\
&+ \lambda_{11}(t)z'(t) \\
&+ \lambda_{12}(t)\big[\alpha[I]fI(t) + \alpha^{'}[I]\gamma VI(t) + \mu[I]N(t)\big] \\
&+ I(t) + B_1c_1^2(t) + B_2c_2^2(t) + \mu_1(z'(t) - c_{max})^2 H_1(z'(t) - c_{max}) \\
&+ \mu_2(z(t) - c_{total})^2 H_2(z(t) - c_{total}) - \sum_{i=1}^{2} \omega_{i1}(t)c_i(t) - \sum_{i=1}^{2} \omega_{i2}(t)(1 - c_i(t)),
\end{aligned}$$

where $z'(t) = c_2(t)(S(t) + E(t) + A(t) + R(t))$ and $\omega_{ij}(t) \geq 0$ are the penalty multipliers satisfying

$$\omega_{i1}(t)c_i(t) = \omega_{i2}(t)(1 - c_i(t)) = 0 \quad \text{at} \quad c_i(t) = c_i^*(t) \quad \text{for} \quad i = 1, 2,$$

with $c_i^*(t) = (c_1^*(t), c_2^*(t))$ is the optimal control pair should be found.

On differentiating the augmented Lagrangian H concerning state variables and setting the result to zero, we get the following adjoint system:

$$\begin{aligned}
\lambda_1^{'}(t) &= -\tfrac{\partial H}{\partial S} \\
&= (\lambda_1(t) - \lambda_2(t))(p(1-c_1(t))(\beta_A A + \beta_I I)) + (\lambda_1(t) - \lambda_{12}(t))\mu[I] \\
&+ (\lambda_1(t) - \lambda_6(t))\psi c_2(t) - c_2(t)\lambda_{11}(t) - 2c_2(t)\mu_1(z'(t) - c_{max})H_1(z'(t) - c_{max}),
\end{aligned}$$

$$\begin{aligned}
\lambda_2^{'}(t) &= -\frac{\partial H}{\partial E} \\
&= \epsilon(\lambda_2(t) - \lambda_3(t)) + (\lambda_2(t) - \lambda_{12}(t))\mu[I] + (\lambda_2(t) - \lambda_7(t))\psi c_2(t) - \lambda_{11}(t)c_2(t) \\
&- 2c_2(t)\mu_1(z'(t) - c_{max})H_1(z'(t) - c_{max}),
\end{aligned}$$

$$\begin{aligned}
\lambda_3^{'}(t) &= -\frac{\partial H}{\partial A} \\
&= p(1-c_1(t)\beta_A S(t)(\lambda_1(t)-\lambda_2(t))+\sigma(\lambda_3(t)-\lambda_4(t))+\mu[I](\lambda_3(t)-\lambda_{12}(t)) \\
&+ \psi c_2(t)(\lambda_3(t)-\lambda_8(t))-c_2(t)\lambda_{11}(t)+b(1-c_1(t))\beta_A V S(t)(\lambda_6(t)-\lambda_7(t)) \\
&- 2c_2(t)\mu_1(z'(t)-c_{max})H_1(z'(t)-c_{max}),
\end{aligned}$$

$$\begin{aligned}
\lambda_4^{'}(t) &= -\frac{\partial H}{\partial I} \\
&= p(1-c_1(t)\beta_I S(t)(\lambda_1(t)-\lambda_2(t))+f(\lambda_4(t)-\lambda_5(t))+\mu[I](\lambda_4(t)-\lambda_{12}(t)) \\
&+ \alpha[I]f(\lambda_5(t)-\lambda_{12}(t))+b(1-c_1)\beta_I V S(t)(\lambda_6(t)-\lambda_7(t))-1,
\end{aligned}$$

$$\begin{aligned}
\lambda_5^{'}(t) &= -\frac{\partial H}{\partial R} \\
&= \mu[I](\lambda_5(t)-\lambda_{12}(t))+\psi c_2(t)(\lambda_5(t)-\lambda_{10}(t))-c_2(t)\lambda_{11}(t) \\
&- 2c_2(t)\mu_1(z'(t)-c_{max})H_1(z'(t)-c_{max}), \\
\lambda_6^{'}(t) &= -\frac{\partial H}{\partial VS} \\
&= b(1-c_1)(\beta_A A(t)+\beta_I I(t))(\lambda_6(t)-\lambda_7(t))+\mu[I](\lambda_6(t)-\lambda_{12}(t)), \\
\lambda_7^{'}(t) &= -\frac{\partial H}{\partial VE} = \epsilon(\lambda_7(t)-\lambda_8(t))+\mu[I](\lambda_7(t)-\lambda_{12}(t)), \\
\lambda_8^{'}(t) &= -\frac{\partial H}{\partial VA} = \sigma(\lambda_8(t)-\lambda_9(t))+\mu[I](\lambda_8(t)-\lambda_{12}(t))+\sigma\delta(\lambda_9(t)-\lambda_{10}(t)), \\
\lambda_9^{'}(t) &= -\frac{\partial H}{\partial VI} = \gamma(\lambda_9(t)-\lambda_{10}(t))+\alpha^{'}[I]\gamma(\lambda_{10}(t)-\lambda_{12}(t))-\mu[I]\lambda_{12}(t), \\
\lambda_{10}^{'}(t) &= -\frac{\partial H}{\partial VR} = \mu[I](\lambda_{10}(t)-\lambda_{12}(t)), \\
\lambda_{11}^{'}(t) &= -\frac{\partial H}{\partial z} = -2\mu_2(z(t)-c_{total})H_2(z(t)-c_{total}), \\
\lambda_{12}^{'}(t) &= -\frac{\partial H}{\partial D} = 0.
\end{aligned}$$

with the transversality conditions $\lambda_i(T) = 0$, for $i = \{1, \ldots, 12\}$. Now, we differentiate the augmented Lagrangian H with respect to $c = (c_1, c_2)$:

$$\begin{aligned}
\frac{\partial H}{\partial c_1} &= (\lambda_1(t)-\lambda_2(t))p(\beta_A A+\beta_I I)S(t)+(\lambda_6(t)-\lambda_7(t))b(\beta_A A+\beta_I I)VS(t) \\
&+ 2B_1c_1(t)-\omega_{11}(t)+\omega_{12}(t).
\end{aligned}$$

$$\begin{aligned}
\frac{\partial H}{\partial c_2} &= -\psi S(t)\lambda_1(t)-\psi E(t)\lambda_2(t)-\psi A(t)\lambda_3(t)-\psi R(t)\lambda_5(t)+\psi S(t)\lambda_6(t)+\psi E(t)\lambda_7(t) \\
&+ \psi A(t)\lambda_8(t)+\psi R(t)\lambda_{10}(t)+(S(t)+E(t)+A(t)+R(t))\lambda_{11}(t)+2B_2c_2(t) \\
&+ 2\mu_1(S(t)+E(t)+A(t)+R(t))(z'(t)-c_{max})H_1(z'(t)-c_{max})-\omega_{21}(t)+\omega_{22}(t).
\end{aligned}$$

Recall that $z'(t) = c_2(t)(S(t)+E(t)+A(t)+R(t))$.

To sum up, we find the optimal control by solving the state system with initial conditions and adjoint equations, we obtain c_1^*, c_2^* defined as:

$$
\begin{aligned}
c_1^* &= \frac{(\lambda_2(t)-\lambda_1(t))p(\beta_A A+\beta_I I)S(t)+(\lambda_7(t)-\lambda_6(t))b(\beta_A A+\beta_I I)VS(t)}{2B_1},\\
&+ \frac{+\omega_{11}(t)-\omega_{12}(t)}{2B_1}\\
c_2^* &= \frac{\psi S(t)(\lambda_1(t)-\lambda_6(t))+\psi E(t)(\lambda_2(t)-\lambda_7(t))+\psi A(t)(\lambda_3(t)-\lambda_8(t))}{2B_2+2\mu_1(S(t)+E(t)+A(t)+R(t))^2H_1}\\
&+ \frac{+\psi R(t)(\lambda_5(t)-\lambda_{10}(t))-(S(t)+E(t)+A(t)+R(t))\Big(\lambda_{11}(t)-2\mu_1 c_{max})H_1\Big)}{2B_2+2\mu_1(S(t)+E(t)+A(t)+R(t))^2H_1}.\\
&+ \frac{\omega_{21}(t)-\omega_{22}(t)}{2B_2+2\mu_1(S(t)+E(t)+A(t)+R(t))^2H_1}.
\end{aligned}
$$

To find an explicit expression for the optimal control without the penalty multipliers ω_{ij}, where $i,j=1,2$, we start the discussion for the first component c_1^* with $c_1 \in [0,1)$ to avoid the case where the force infection $\lambda=0$ (case where $c_1=1$). For that, we consider the following cases:

Case 1: On the set $\{t|0<c_1^*(t)<1\}$, we have $\omega_{11}(t)=\omega_{12}(t)=0$. Hence the optimal control c_1^* becomes

$$
c_1^* = \frac{(\lambda_2(t)-\lambda_1(t))p(\beta_A A+\beta_I I)S(t)+(\lambda_7(t)-\lambda_6(t))b(\beta_A A+\beta_I I)VS(t)}{2B_1}.
$$

Case 2 : On the set $\{t|c_1^*(t)=0\}$, we have $\omega_{12}(t)=0$ and $\omega_{11}(t)\geq 0$. Hence

$$
c_1^* = \frac{(\lambda_2(t)-\lambda_1(t))p(\beta_A A+\beta_I I)S(t)+(\lambda_7(t)-\lambda_6(t))b(\beta_A A+\beta_I I)VS(t)+\omega_{11}(t)}{2B_1},
$$

which implies that

$$
c_1^* = \frac{(\lambda_2(t)-\lambda_1(t))p(\beta_A A+\beta_I I)S(t)+(\lambda_7(t)-\lambda_6(t))b(\beta_A A+\beta_I I)VS(t)}{2B_1} \leq 0.
$$

Combining these two cases, the optimal control c_1^* is characterized as

$$
c_1^* = \min\Big[1, \max\Big\{0, \frac{(\lambda_2(t)-\lambda_1(t))p(\beta_A A+\beta_I I)S(t)+(\lambda_7(t)-\lambda_6(t))b(\beta_A A+\beta_I I)VS(t)}{2B_1}\Big\}\Big]. \tag{4.16}
$$

We proceed with the same reasoning to find c_2^*, where $c_2 \in [0,1]$ and we add the following third case:

Case 3: On the set $\{t|c_2^*(t)=1\}$, we have $\omega_{21}(t)=0$ and $\omega_{22}(t)\geq 0$. Hence

$$
\begin{aligned}
1 &= c_2^*\\
&= \frac{\psi S(t)(\lambda_1(t)-\lambda_6(t))+\psi E(t)(\lambda_2(t)-\lambda_7(t))+\psi A(t)(\lambda_3(t)-\lambda_8(t))}{2B_2+2\mu_1(S(t)+E(t)+A(t)+R(t))^2H_1}\\
&+ \frac{+\psi R(t)(\lambda_5(t)-\lambda_{10}(t))-(S(t)+E(t)+A(t)+R(t))\Big(\lambda_{11}(t)-2\mu_1 c_{max})H_1\Big)-\omega_{22}(t)}{2B_2+2\mu_1(S(t)+E(t)+A(t)+R(t))^2H_1},
\end{aligned}
$$

which implies that

$$\begin{aligned} c_2^* &= \frac{\psi S(t)(\lambda_1(t)-\lambda_6(t))+\psi E(t)(\lambda_2(t)-\lambda_7(t))+\psi A(t)(\lambda_3(t)-\lambda_8(t))}{2B_2+2\mu_1(S(t)+E(t)+A(t)+R(t))^2H_1} \\ &+ \frac{+\psi R(t)(\lambda_5(t)-\lambda_{10}(t))-(S(t)+E(t)+A(t)+R(t))\Big(\lambda_{11}(t)-2\mu_1 c_{max})H_1\Big)}{2B_2+2\mu_1(S(t)+E(t)+A(t)+R(t))^2H_1} \\ &+ \frac{\omega_{21}(t)-\omega_{22}(t)}{2B_2+2\mu_1(S(t)+E(t)+A(t)+R(t))^2H_1} \geq 1. \end{aligned}$$

To conclude, we get

$$\begin{aligned} c_2^* = \min\Big[1, \max\Big\{0, &\frac{\psi S(t)(\lambda_1(t)-\lambda_6(t))+\psi E(t)(\lambda_2(t)-\lambda_7(t))+\psi A(t)(\lambda_3(t)-\lambda_8(t))}{2B_2+2\mu_1(S(t)+E(t)+A(t)+R(t))^2H_1} \\ &+ \frac{\psi R(t)(\lambda_5(t)-\lambda_{10}(t))-(S(t)+E(t)+A(t)+R(t))\Big(\lambda_{11}(t)-2\mu_1 c_{max})H_1\Big)}{2B_2+2\mu_1(S(t)+E(t)+A(t)+R(t))^2H_1}\Big\}\Big]. \end{aligned} \tag{4.17}$$

The optimal control (c_1^*, c_2^*) satisfies this problem (4.14) as well as the corresponding optimal solutions for the system (2.1). Furthermore, due to the boundedness of the solutions for the state and adjoint variables, the Lipschitz properties of the systems (2.1) and the transversality conditions $\lambda_i(T) = 0$, for $i = \{1, \ldots, 12\}$, as well as the equations (4.16), (4.17) that defines the control, it is possible to establish the uniqueness of this control.

5 Numerical simulations and discussion

In this section, we perform numerical simulations for a previous model to estimate the evolution of the COVID-19 outbreak in France. The simulations focus on solving a constrained optimal control problem applied to vaccination. The problem is solved numerically with Python using the fourth-order Runge-Kutta optimization method. The values of the model parameters are obtained from available local data and previous studies.

The simulations consider the period before the vaccination program in France, as well as the period after vaccination. Figures are presented to illustrate the simulation results, including the number of infected individuals and the number of deaths. The impact of control measures and vaccination on the spread of the infection and the reduction of deaths is analyzed.

Overall, the simulations provide insights into the effectiveness of vaccination and control measures in managing the COVID-19 outbreak in France.

5.1 Model state variables and parameters

Table 1 provides a summary of the model's state variables and parameters. The state variables include the densities of susceptible, vaccine susceptible, latent, vaccine latent, asymptomatic infectious, vaccine asymptomatic infectious, symptomatic infectious, vaccine symptomatic infectious, recovered individuals, vaccine recovered individuals and total deaths. The parameters include the basic reproduction number, proportion of infections, proportion of infections vaccinated, proportion of recovery among vaccinated, transmission rates, reduced transmission factor of infections, control effort, immigration rate, waiting rates to viral shedding and symptom onset, recovery rates from infections, natural mortality rate, disease-induced mortality rates, healthcare capacity, cost weight, and initial conditions. The best-fit values of these parameters were obtained from [9] and the available local data.

Table 1. Model state variables and parameters

Variables	Description
S, VS	Density of susceptible and susceptible vaccinated individuals
E, VE	Density of latent and latent vaccinated individuals
A, VA	Density of asymptomatic and asymptomatic vaccinated infectious individuals
I, VI	Density of symptomatic and symptomatic vaccinated infectious individuals
R, VR	Density of recovered and recovered vaccinated individuals
D	Total deaths

Parameters	Description (unit)	Value(range) [ref.]
p	Proportion of infections	$0.9(0.85 - 0.95)$[9]
β_I	Symptomatic transmission rate	Calculated [a]
β_A	Asymptotic transmission rate	Calculated [a]
b	Proportion of infections vaccinated individuals	0.2 [assumed]
c_1	Control public health effort	$(0, 1)$
c_2	Control effort due to the vaccination	(0,1)
ε	Waiting rate to viral shedding (day $^{-1}$)	$1/4.2(0.21 - 0.27)$[16]
σ	Waiting rate to symptom onset (day $^{-1}$)	$1(0.9 - 1.1)$[7]
f	Recovery rate (day $^{-1}$)	1/17 [assumed]
γ	Recovery rate from infections (day $^{-1}$)	$1/15(0.067 - 0.1)$[27]
δ	proportion of recovered among vaccine asymptomatic	0.8 [assumed]
μ	Natural mortality rate with hospital saturation (day $^{-1}$)	10^{-5} [assumed]
Λ	Recruitment rate in the population	μN_0 [assumed]
$\alpha_{\min}$	Lower bound disease-induced mortality rate (day $^{-1}$)	Calculated [a]
$\alpha_{\max}$	Higher bound induced mortality rate $\left(\text{day}^{-1}\right)$	$2\alpha_{\min}$ [assumed]
I^*	Healthcare capacity	120000 [assumed]
B_1, B_2	Cost weight	$800(0, \infty)$ [assumed]
Initial conditions		
N_0	Total population	67×10^6
I_0	Size of infected population	$0.01 \times I^*$(variable)
S_0	Size of susceptible population	$N_0 - I_0$

[a] The parameters $\alpha_{\min}, \beta_I, \beta_A$ are calculated by Djidjou-Demasse et al., see [9].

5.2 SEAIR model before vaccination

First, we consider the model (1) before the vaccine deployment, during the period from December 2020 through May 2021, in France. We assume that the vaccinated sub-populations, VS, VE, VA, VI and VR are equal to zero. We use the Runge Kutta scheme to solve the set of differential equations.

For simplicity and straightforward analysis of causality, we take initial conditions

$$\begin{aligned} I_0 &= 6458, \\ E_0 &= 2 \times 6458, \\ A_0 &= 1.5 \times 6458, \\ S_0 &= N_0 - (I_0 + E_0 + A_0 + R_0 + D_0), \\ R_0 &= VS_0 = VE_0 = VA_0 = VI_0 = VP_0 = VR_0 = 0, \\ D_0 &= 34. \end{aligned}$$

In the following Figure 2, each color corresponds to one of the compartments of the model (Susceptible, Latent, Asymptomatic, Infected, Recovered, and Death).

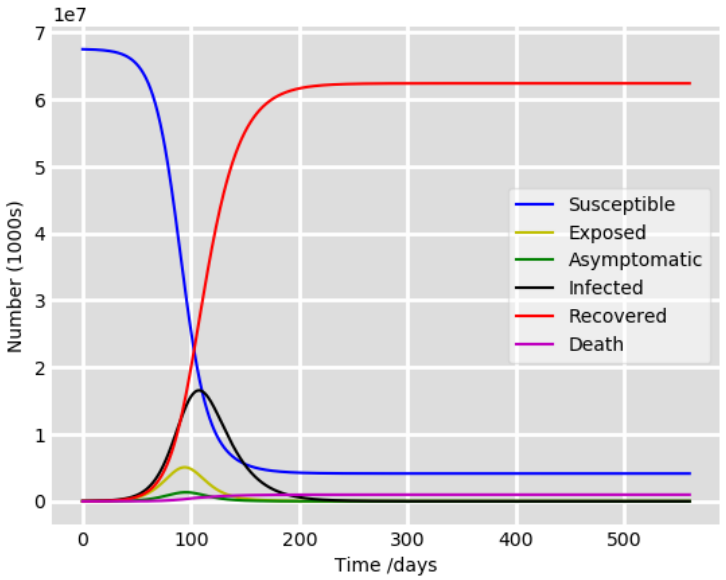

Figure 2. The model simulation before the vaccination program in France

We can see that in the absence of any control, the number of infected individuals grows exponentially fast at the beginning of the epidemic (curve in black color) and the epidemic reaches its peak, the equilibrium point as the intersection of the curves for those still susceptible and those immunized following recovery, 110 days after the beginning.

This is the natural behavior of an epidemic. However, waiting for a large part of the population to become infected to mitigate the epidemic is certainly not the best strategy, especially when the disease presents high mortality due to the severity of the infection or the saturation of the healthcare system.

In the following section, we will simulate the solutions of the extended SEAIR model (1) to estimate the impact of the vaccination program in France.

5.3 Vaccination effect in France and discussion

We will now simulate the solution to the model (1) to assess the impact of the vaccination program to combat the infectious diseases caused by COVID-19. The first dose of the COVID-19 vaccine in France was received for the first time on December 27, 2020. Since then, the number of doses has multiplied rapidly to protect the population as quickly as possible.

Table 2. Distribution of vaccine in France

Vaccines used	Efficiency rate (ψ)	Administered doses
Pfizer	95%	81 490 504
AstraZeneca/Oxford	70%	7 838 931
Moderna	50.38%	12 357 533
Johnson and Johnson	66%	1 074 197

Table 2 provides an overview of the distribution of vaccines in France, highlighting their efficacy rates.

In the numerical simulations, we compare the optimal intervention strategies under different settings of a proportion of infections, waiting rate to viral shedding, symptom onset, and the infection rate among vaccines. In France, these results are given for the period from February 15, 2021, to April 30, 2021, when the number of cases goes past 50000 infected cases (Figure 3). Vaccination is highly concentrated.

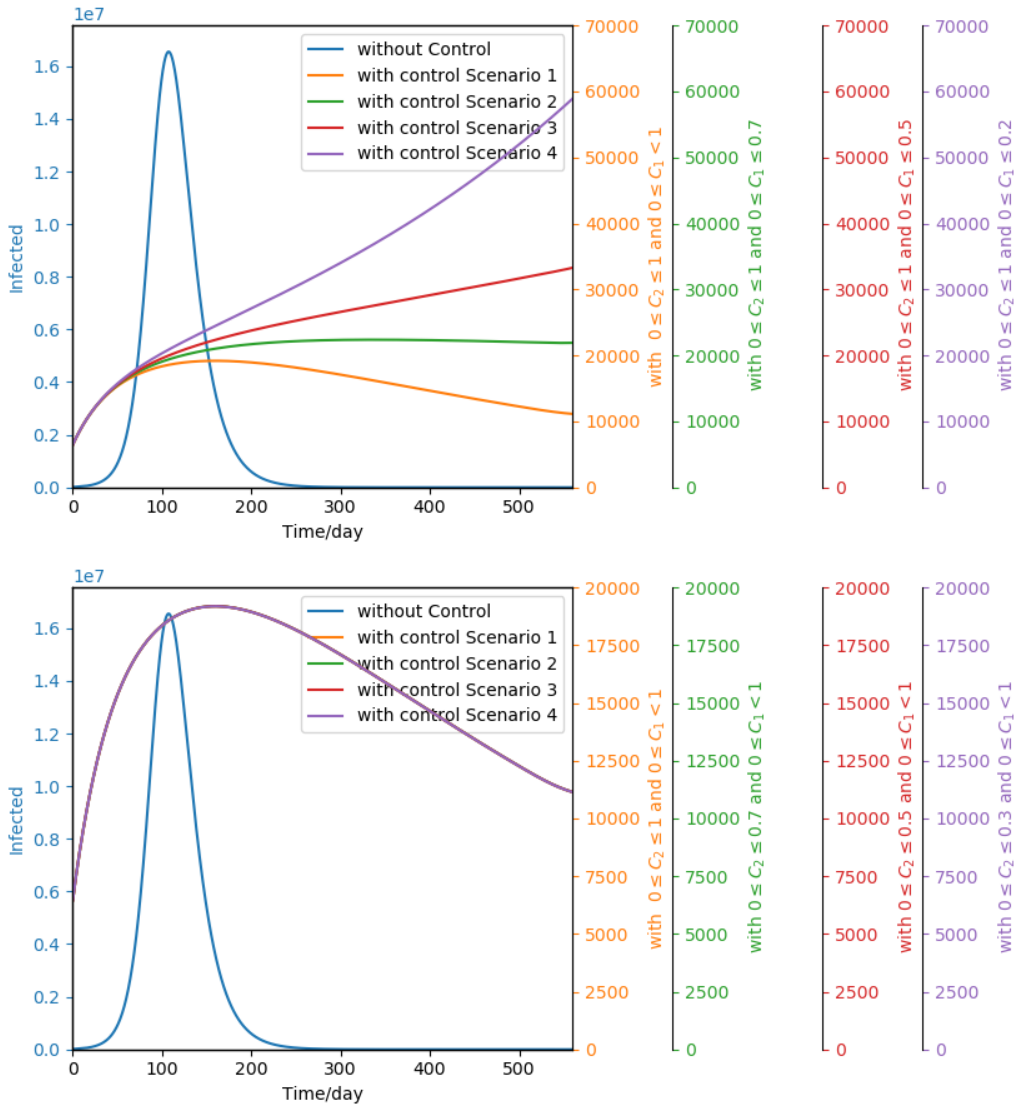

Figure 3. Comparison infected people in France before and after vaccination

From Figure 3, we can observe that the number of infected individuals is influenced by the control parameter of the measures taken to control the spread of diseases c_1. Without control measures, the number of infected individuals exceeds 16 million (1.6e7). Under the optimal vaccination, the spread of infection is significantly reduced in Scenario 1 when c_1 and c_2 range between 0 and 1, resulting in a lower rate of new infections.

Furthermore, they show a clear correlation between an increase in the maximum vaccination threshold and a significant reduction in the peak of critical infections. This underlines the importance of achieving high vaccination coverage rates to mitigate the spread of infectious diseases and protect vulnerable populations

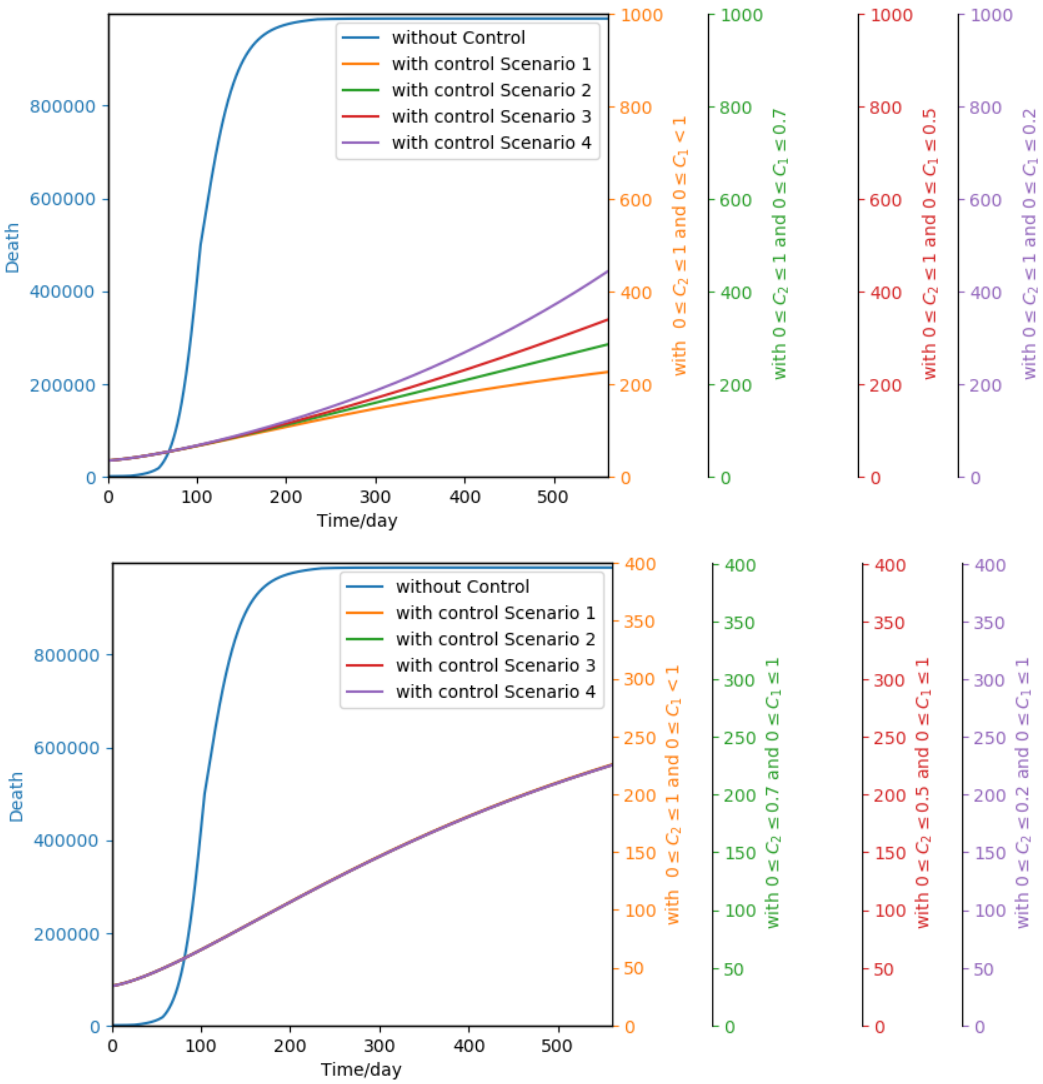

Figure 4. Comparison between death people in France before and after vaccination

In this optimal case, the improved control measures impact the number of infected individuals and influence the number of deaths, illustrated in Figure 4. By implementing the optimal control measures in scenario 1, the number of deaths is expected to be reduced to 205 compared to the other scenarios.

Figure 3 and 4 compare the scenarios with and without control. In the no-control scenario, no prevention or control measures are implemented. The number of infections quickly peaks, which can lead to the overloading of the healthcare system and the rapid spread of disease within the population. In other scenarios, control measures are applied and the peak number of infections is reduced compared to the uncontrolled scenario but remains relatively high. This may include the importance of measures such as social distancing, wearing masks, or the quarantine presented by c_1, which may give different results when increased. For the first scenario, this is the best possible situation regarding control. The number of infections remains low throughout the period studied, thanks to effective prevention measures and a rapid response to new cases.

Thus, the higher the number of infections, the higher the value of the infection severity indicator. Furthermore, if the infection's capacity to spread is lower, this could indicate a slower spread. Finally, a higher value for healing capacity or mortality may mean better healing or lower mortality.

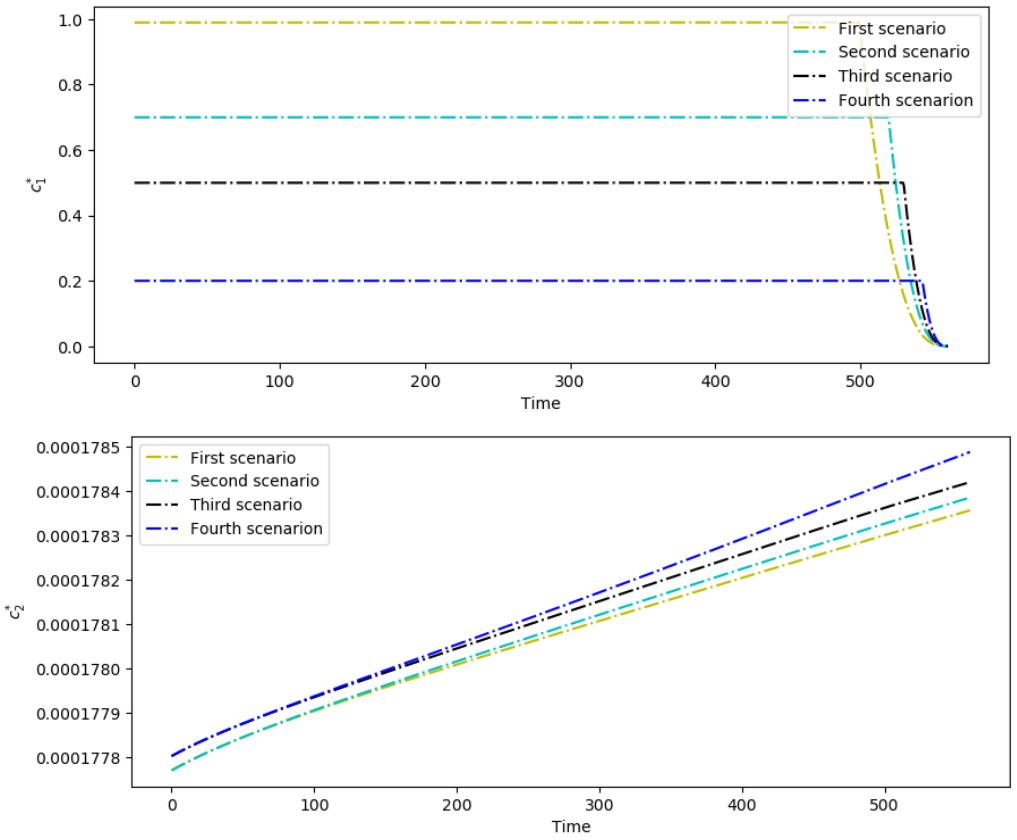

Figure 5. Progression of the optimal controls c_1^* and c_2^* over time.

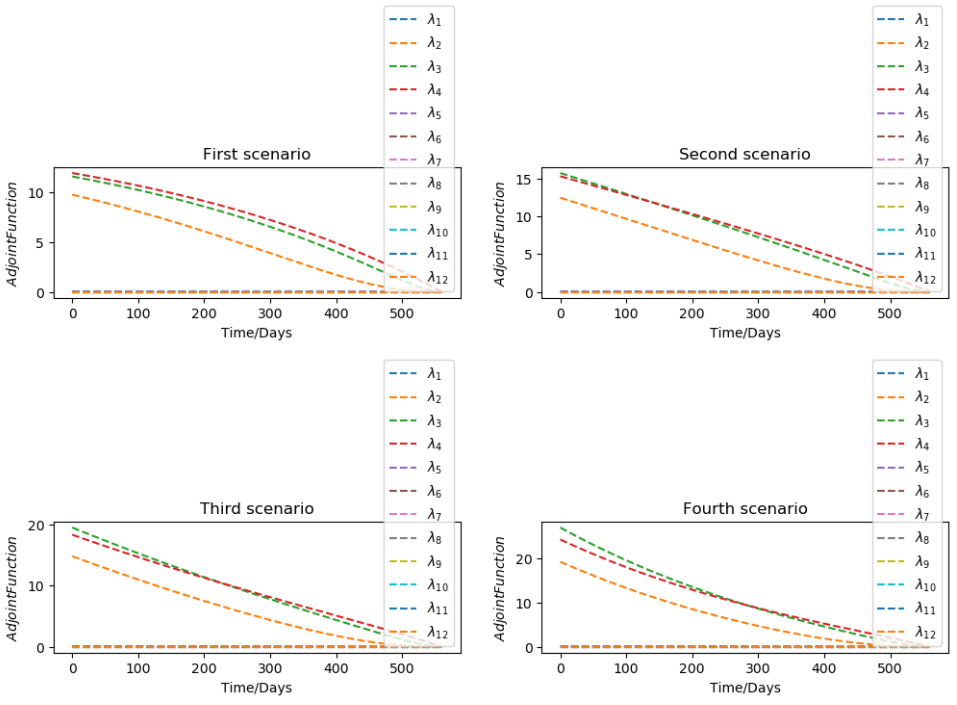

Figure 6. Adjoint Function

Figure 5 shows the progression of optimal controls c_1^* and c_2^* over time. For all four scenarios,

we observe that control c_1^*, defined by the percentage reduction in transmission due to a public health measure or sanitary control at time t, always takes the maximum that is described in equation (4.16) this shows the necessity of sanitary restraint to the extinction of the epidemic.

Whereas for the c_2^* control, which measures the rate at which individuals are vaccinated, we observe that the curves for the different scenarios are characterized by low and almost constant growth throughout the vaccination period (between $1.778e-04$ and $1.785e-04$), indicating that the optimal vaccination strategy is to vaccinate all individuals simultaneously when total coverage is possible.

Figures 6 describe the evolution of the adjoint functions λ_i, $i \in \{1, \ldots, 12\}$ weights of the Lagrangian to control the relative importance of constraints compared to the objective function J_p during the optimization problem-solving.

Figure 7 shows three vaccination scenarios over time (in days). The maximum value is around 20000, but decreases over time. The more effective the vaccination strategy, the lower the number of infected people.

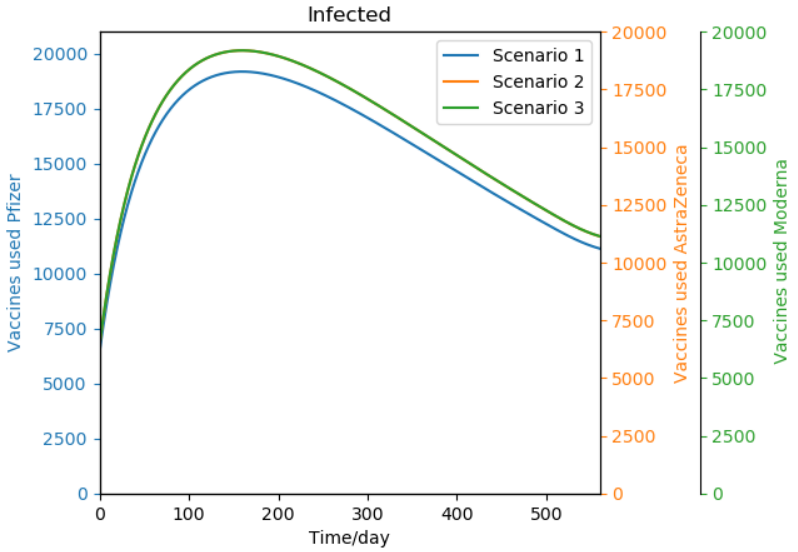

Figure 7. Comparison of infections with different efficacy rates in France

COVID-19 vaccines have proven to be safe, effective, and life-saving. Like all vaccines, they do not fully protect everyone who is vaccinated. Figure 7 shows that Pfizer reduces the number of infected people compared to Moderna and AstraZeneca, but all vaccines achieve the same goal.

5.4 Impact of constant vaccination, restriction measures, and transmission rate on $\mathcal{R}_0$

Using the basic reproduction number $\mathcal{R}_0$ (3.2), we study the influence of vaccination (c_2), restrictive measures (c_1) and transmission rates (β_I, β_A) on epidemic dynamics.

In Figures 8 and 9, the curves illustrate the variation of the basic reproductive number $\mathcal{R}_0$ as a function of the transmission rates β_A and β_I. Each curve corresponds to one of four scenarios, characterized by distinct values of the vaccination rate (c_2) and the restraint rate (c_1). When $\mathcal{R}_0$ varies as a function of β_A, the transmission rate β_I is fixed at 2.2937×10^{-9}. Conversely, when $\mathcal{R}_0$ varies as a function of β_I, the transmission rate β_A is fixed at 4.5874×10^{-9}.

When c_1 varies between 25% and 90% and β_I ranges from 0 to 1.4×10^{-8}, with no vaccination $c_2 = 0$, the effect of c_1 directly manifests as a reduction in the numerator via the factor $(1 - c_1)$, leading to a decrease in $\mathcal{R}_0$. Furthermore, an increase in β_I amplifies the transmission between asymptomatic and symptomatic individuals through the $\beta_A \epsilon(f + \mu[I]) + \beta_I \epsilon \sigma$, as illustrated in the figure 9.

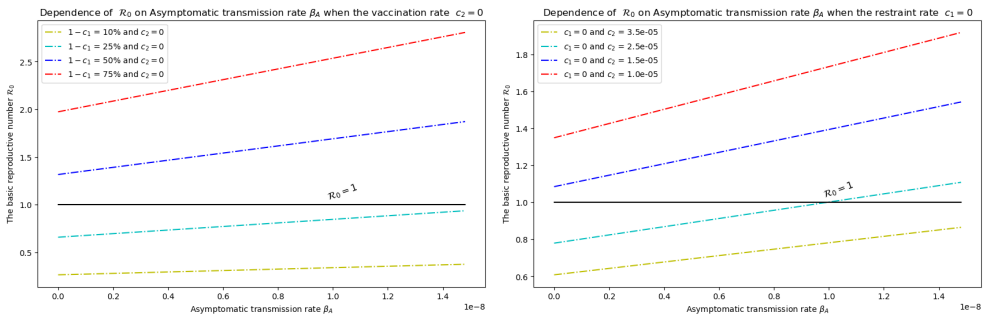

Figure 8. Impact of asymptomatic transmission rate (β_A) and public health effort rate (c_1 constant) and vaccination rate (c_2 constant) on the basic reproduction number ($\mathcal{R}_0$).

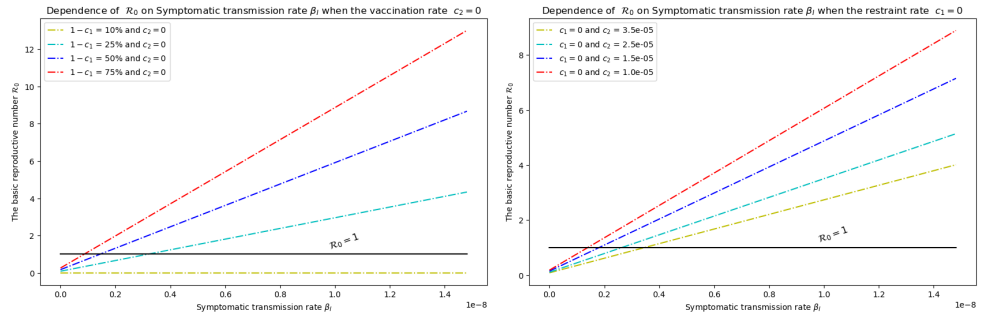

Figure 9. Impact of symptomatic transmission rate (β_I) and vaccination rate (c_2 constant) on the basic reproduction number ($\mathcal{R}_0$).

At $c_1 = 75\%$, $\mathcal{R}_0$ plateaus around 4 when $\beta_I = 1.4 \times 10^{-8}$, indicating a strong transmission rate and revealing the saturation of restriction effectiveness. For $\beta_I > 0.2 \times 10^{-8}$, a restriction level of at least $c_1 \geq 75\%$ is required to maintain $\mathcal{R}_0 < 1$.

For a given value of β_A, increasing c_2 (which reflects a higher vaccine efficacy) reduces $\mathcal{R}_0$. For example, when $\beta_A = 0.8 \times 10^{-8}$, increasing c_2 from 2.5×10^{-5} to 3.5×10^{-5} causes $\mathcal{R}_0 < 1$, whereas a lower value of $c_2 = 1.0 \times 10^{-5}$ results in $\mathcal{R}_0 \approx 1.7$. Thus, effective epidemic control $\mathcal{R}_0 < 1$ is only achievable when vaccine efficacy is sufficiently high and strict public health restrictions are simultaneously enforced.

At a high vaccination level ($c_2 \approx 2.5 \times 10^{-5}$), the basic reproduction number $\mathcal{R}_0$ approaches 1 for $\beta_A = 1.0 \times 10^{-8}$, indicating a near-containment scenario. For $\beta_A > 0.8 \times 10^{-8}$, maintaining $c_2 \geq 2.5 \times 10^{-5}$ is necessary to prevent $\mathcal{R}_0$ from exceeding 1 [30]. When both restriction levels (c_1) and vaccination coverage (c_2) are low, high transmission rates ($\beta_I \geq 0.2 \times 10^{-8}$ or $\beta_A \geq 1.0 \times 10^{-8}$) lead to $\mathcal{R}_0 > 1$, resulting in uncontrolled epidemic surges. In contrast, a combination of strict public health measures ($c_1 = 75\%$) and high vaccination coverage ($c_2 \geq 2.5 \times 10^{-5}$) effectively reduces $\mathcal{R}_0$ below the critical threshold of 1, even under high transmission conditions. Two distinct dynamical regimes emerge: in a subcritical bifurcation, where $\mathcal{R}_0 < 1$, small parameter variations (e.g., a 10% decrease in c_1) do not trigger outbreaks. Conversely, in a supercritical bifurcation, when $\mathcal{R}_0 > 1$ even minor increases in transmission rates ($\beta_A = 4.5874 \times 10^{-9}$) lead to exponential growth in infections (figure 9).

Asymptomatic transmission β_A is dominant in determining R_0, particularly critical for pathogens, where 30–50% of transmissions occur asymptomatically. This highlights the necessity of targeted testing to mitigate undetected spread [16]. The vaccination rate c_2 not only reduces the susceptible population S^* but also slows disease progression by influencing the rates $(\epsilon + \mu[I] + \psi c_2)$, providing a dual protective effect. A high vaccination rate (c_2) can compensate for lower restriction measures (c_1), effectively controlling transmission.

Table 3. Public Health Implications

Scenario	Optimal Policy	Target
High β_A	Prioritize $c_2 \geq 2.5 \times 10^{-5}$	Reduce asymptomatic reservoir
High β_I	Enforce $c_1 \geq 75\%$, test symptomatic cases	Suppress symptomatic spread
Variant Emergence	Boost c_2, temporary $c_1 \uparrow 30\%$	Maintain $\mathcal{R}_0 < 1$

Table 3 outlines a set of recommended public health measures in response to the observed effects of asymptomatic and symptomatic transmission on $\mathcal{R}_0$. These measures align with our findings, suggesting targeted strategies to mitigate epidemic spread under different transmission scenarios. Specifically, the proposed policies emphasize vaccination efforts to control asymptomatic reservoirs, stringent symptomatic case detection to curb symptomatic transmission, and adaptive interventions in response to variant emergence.

6 Conclusion

In this work, we studied a mathematical model for COVID-19 with vaccination. Our work was based on the SEAIR model proposed in [9] by incorporating vaccinated compartments. We have analyzed the existence and uniqueness of the solution and shown that our model has two equilibrium states, and we have calculated the reproduction number $\mathcal{R}_0$. Furthermore, we determined a condition that guarantees the local asymptotic stability of the equilibrium points.

We focused on this frame to address the following question: in a context where vaccines are deployed and maintained under public restriction, how can we best allocate the control effort for the epidemic over the necessary period? Using optimal control theory, we showed that, assuming a quadratic cost for the control effort at a given time $(c_1(t), c_2(t))$ associated respectively with public health restrictions and vaccination effectiveness, an optimal control strategy significantly reduces the number of infected individuals.

We formulated an optimal control problem integrating two realistic constraints, considering the limited vaccination coverage and maximum daily vaccine administration, and used the conditions of the Filippov-Cesari existence theorem to characterize the optimal control. Unconstrained problems are formed by adding to the objective function a penalty function.

Then, we numerically solved the model for the COVID-19 pandemic in France using parameters developed in the literature. The optimal strategy was verified under different scenarios: health restrictions limited to 20, 50, 75, and 100 percent. The results suggest starting vaccination at the same time, whatever the current constraints.

Our results show that higher maximum c_1^* restriction rates reduce the number of severely infected people in all countries, but do not lead to a slight reduction in infection. We therefore recommend the mandatory introduction of parallel vaccination for all populations, as the only way to reduce mortality.

In conclusion, this study provides valuable information on the optimal vaccination control strategy and public health measures. The results may help in making decisions aimed at reducing the number of people infected and mortality caused by infectious diseases.

In future research, incorporating stochastic perturbations can enhance SEAIR models by accounting for uncertainties and variabilities in vaccination rates, efficacy, and public response. Specifically, the transmission coefficient, which depends on regional behavior and daily life, can be influenced by randomness. This can be achieved by perturbing the coefficient itself or by adding stochastic perturbations proportional to model parameters such as susceptible (S), exposed (E), asymptomatic (A), and infected (I) individuals. These adjustments allow for a more robust and realistic representation of epidemic dynamics.

References

[1] **A. Aghriche.** *Mathematical model of COVID-19 transmission with education campaign and treatment through quarantine*, Palestine Journal of Mathematics Vol 14(1), 142–154, (2025).

[2] **Z. Ahmad, G. Bonanomi, D. Di Serafino, F. Giannino.** *Transmission dynamics and sensitivity analysis of pine wilt disease with asymptomatic carriers via fractal-fractional differential operator of Mittag-Leffler kernel*, Applied Numerical Mathematics Volume 185, pp. 446-465, Elsevier (2023).

[3] **Z. Ahmad et al.** *A global report on the dynamics of COVID-19 with quarantine and hospitalization: A fractional order model with non-local kernel*, SComputational Biology and Chemistry Volume 98, 107645, Elsevier (2022).

[4] **Z. Ahmad, M. Arif, F. Ali, et al.** *A report on COVID-19 epidemic in Pakistan using SEIR fractional model*, Sci Rep 10, 22268 (2020).

[5] **H. Amann**, *Ordinary Differential Equations: An Introduction to Nonlinear Analysis (Degruyter Studies in Mathematics)*, Walter De Gruyter Inc, (1990).

[6] **D. Aldila, M. Shahzad, S.H.A. Khoshnaw, M. Ali, F. Sultan , A. Islamilova, Y. R. Anwar, B.M. Samiadji .** *Optimal control problem arising from COVID-19 transmission model with rapid-test*, Restults in Physics, volume 37, (2020).

[7] **L. Cesari.** *Optimization Theory and Applications: Problems with Ordinary Differential Equations.* Springer-Verlag, New York, (1983).

[8] **J. Danane, K. Allali, Z. Hammouch, K. S. Nisar.** *Mathematical analysis and simulation of a stochastic COVID-19 Levy jump model with isolation strategy.* Results in Physics, 23-103994, Elsevier (2021).

[9] **R. Djidjou Demasse, Y. Michalakis, M. Choisy, M. T. Sofonea, S. Alizon.** *Optimal COVID-19 epidemic control until vaccine deployment.* medRxivl. Cold Spring Harbor Laboratory Press (2020).

[10] **M. H. FARAG.** *On an optimal control constrained problem governed by parabolic type equations* . Palestine Journal of Mathematics. Vol. 4(1) , 136–143, (2015).

[11] **H. Gaff, E. Schaefer.** *Optimal control applied to vaccination and treatement strategies for various epidemiological models* Mathematical biosciences and engineering, Volume 6, Number 3, (2009).

[12] **X. He, et al.** *Temporal dynamics in viral shedding and transmissibility of COVID-19.* Nature Medicine, 26(5), 672-675. DOI: 10.1038/s41591-020-0869-5, (2020).

[13] **I.M. Hezam, A. Foul, A. Alrasheedi.** *A dynamic optimal control model for COVID-19 and cholera coinfection in Yemen.* Advances in Difference Equations, 2021:108, SpringerOpen Journal (2021).

[14] **D.M. Himmelblau.** *Applied Nonlinear Programming* , McGraw-HiLl, New York, (1972).

[15] **J. Kim, H.D. Kwon, J. Lee.** *Constrained optimal control applied to vaccination for influenza.* Computers and Mathematics with Applications V. 71, Issue 11, pp. 2313-2329 (2016).

[16] **R. Li, et al.** *Substantial undocumented infection facilitates the rapid dissemination of novel coronavirus (SARS-CoV-2).* Science, 368(6490), 489-493. DOI: 10.1126/science.abb3221 (2020).

[17] **U. Ledzewicz, H. Schattler.** *On optimal control for a general SIR-model with vaccination ans treatment* Discrete and continuous Dynamical systems, (2011).

[18] **S. L. Lenhart, J. T. Workman.** *Optimal Control Applied to Biological Models,* Chapman Hall/CRC, (2007).

[19] **M. Y. Li.** *An introduction to mathematical modeling of infectious diseases* (Vol. 2). Cham, Switzerland: Springer (2018).

[20] **F. Lin, , K. Muthuraman, M. Lawley.** *An optimal control theory approach to non-pharmaceutical interventions.* BMC Infect Dis 10(1):32. (2010).

[21] **Q. Lin, S. Zhao, D. Gao, Y. Lou, et al.** *A conceptual model for the coronavirus disease 2019 (COVID-19) outbreak in Wuhan, China with individual reaction and governmental action* International Journal of Infectious Diseases 93, 211-216, (2020).

[22] **Z. Liu, P. Magal, O. Seydi, and G. Webb.** *Understanding Unreported Cases in the COVID-19 Epidemic Outbreak in Wuhan, China, and the Importance of Major Public Health Interventions.* Biology, (2020).

[23] **D.G. Luenberger, Y. Ye.** *Linear and Nonlinear Programming, Vol. 116* Springer Science and Business Media (2008).

[24] **A. Malik, M. Alkholief, F.M. Aldakheel et al.** *Sensitivity analysis of COVID-19 with quarantine and vaccination: A fractal-fractional model.* Alexandria Engineering Journal, Volume 61, Issue 11, pp. 8859-8874 (2022).

[25] **B. Naffeti, W. Ben Aribi, et al.** *Comparative reconstruction of SARS-CoV-2 transmission in three African countries using a mathematical model integrating immunity data.* IJID Regions Volume 10, Pages 100-107 (2024).

[26] **D. P. Oran, E. J. Topol.** *Prevalence of asymptomatic SARS-CoV-2 infection.* Annals of Internal Medicine, 173(5), 362-367. DOI: 10.7326/M20-3012 (2020).

[27] **A.G.C. Perez, D.A. Oluyori.** *An extended SEIARD model for COVID-19 vaccination in Mexico: analysis and forecast.* Mathematics in Applied Sciences and Engineering doi: 10.5206-14233 (2021).

[28] **S. Lenhart, J. Workman.** *Optimal Control Applied to Biological Models,*. New York: Chapman and Hall, (2007).

[29] **T. A. Perkins, G. Espana.** *Optimal Control of the COVID-19 Pandemic with Non-pharmaceutical Interventions.* Bulletin of Mathematical Biology 82:118, Society for Mathematical Biology (2020).

[30] **Dagan, Noa & al.** *BNT162b2 mRNA Covid-19 Vaccine in a Nationwide Mass Vaccination Setting.* The New England journal of medicine vol. 384,15 (2021): 1412-1423. doi:10.1056/NEJMoa2101765

[31] **L.S. Pontryagin, V.G. Boltyanskii, R.V. Gamkrelidze, E.F. Mishchenko.** *The Mathematical Theory of Optimal Processes* Vol. 528, Interscience Publishers John Wiley and Sons, Inc., New York-London, p. 28. (1962)

[32] **K. Shah et al.** *Fractional Unraveling pine wilt disease: Comparative study of stochastic and deterministic model using spectral method*, Expert Systems with Applications Volume 240, 122407, Elsevier (2024).

[33] **M. Sinan et al.** *Fractional order mathematical modeling of typhoid fever disease*, Results in Physics 32, 105044, Elsevier (2022).

[34] **J. A. Snyman, C. FP.Angos AND Y. Yavin.** *Penalty function solutions to optimal control problems with general constraints via a dynamic optimasition method*, Computers Math. Applic. Vol. 23, No. 11, pp. 47-55, (1992).

[35] **J.H. Tanne, E. Hayasaki, M. Zastrow, P. Pulla, P. Smith, A.G. Rada.** *Covid-19: how doctors and healthcare systems are tackling coronavirus worldwide*, the BMJ, (2020).

[36] **A. Tesfay, T. Saeed, A. Zeb, D. Tesfay, A. Khalaf, J. Brannan.** *Dynamics of a stochastic COVID-19 epidemic model with jump-diffusion.* Advances in Difference Equations, 2021:228, SringerOpen journal (2021).

[37] **P. Van den Driessche, J. Watmough.** *Reproduction numbers and sub-threshold endemic equilibria for compartmental models of disease transmission*. Math. Biosci. 180(1-2), 29-48 (2002).

Author information

Chiraz Trabelsi, Département de Sciences et Technologies, Université de Mayotte.
Institut Montpélliérain Alexander Grothendieck, UMR CNRS 5149, Université de Montpellier, France.
E-mail: chiraz.trabelsi@univ-mayotte.fr
chiraz.trabelsi@umontpellier.fr

Rim Amami, Department of Basic Sciences, Deanship of Preparatory Year and Supporting Studies, Imam Abdulrahman Bin Faisal University, P.O. Box 1982, Dammam 3421, Saudi Arabia.
E-mail: rabamami@iau.edu.sa

Walid Ben Aribi, Esprit School of Business.
University of Tunis El Manar, Pasteur Institute of Tunis, LR16IPT09 Bio-(Informatics, Mathematics and Statistics) Lab, Tunis, Tunisia.
E-mail: ben.aribi.walid89@gmail.com

Hani Abidi, Esprit School of Business.
LR11ES13, Research Laboratory for Mathematical Modeling, Statistical Reliability, and Stochastic Analysis, Tunisia.
E-mail: abidiheni@gmail.com

Received: 2024-12-10
Accepted: 2025-06-28